

云南毛坪大型铅锌矿床成矿物质来源: 原位 S 和 Pb 同位素制约^{*}

谈树成¹ 周家喜^{1,2**} 罗开^{2,3} 向震中^{2,3} 何小虎¹ 张亚辉¹

TAN ShuCheng¹, ZHOU JiaXi^{1,2**}, LUO Kai^{2,3}, XIANG ZhenZhong^{2,3}, HE XiaoHu¹ and ZHANG YaHui¹

1. 云南大学资源环境与地球科学学院, 昆明 650500

2. 中国科学院地球化学研究所, 矿床地球化学国家重点实验室, 贵阳 550081

3. 中国科学院大学, 北京 100049

1. School of Resource Environment and Earth Sciences, Yunnan University, Kunming 650500, China

2. Stake Key Laboratory of Ore Deposit Geochemistry, Institute of Geochemistry, Chinese Academy of Sciences, Guiyang 550081, China

3. University of Chinese Academy of Sciences, Beijing 100049, China

2018-08-15 收稿, 2019-02-15 改回.

Tan SC, Zhou JX, Luo K, Xiang ZZ, He XH and Zhang YH. 2019. The sources of ore-forming elements of the Maoping large-scale Pb-Zn deposit, Yunnan Province: Constrains from in-situ S and Pb isotopes. *Acta Petrologica Sinica*, 35(11): 3461–3476, doi: 10.18654/1000-0569/2019.11.13

Abstract The Sichuan-Yunnan-Guizhou Pb-Zn metallogenic province, located in the western margin of the Yangtze Block, is one of the important bases for the production of base metals in China. The Maoping large-scale Pb-Zn deposit, occurred in the middle of this province, is the second largest Pb-Zn deposit. Its proven total Pb and Zn metal reserves exceed 3Mt, and the average grade of Pb + Zn is 12% ~ 30%, with a local reach of 45%. The ore bodies occur as a layered, lenticular or veined shape distributed in the NW inverted wing of the Maomaoshan anticline and its inclined end NE interlay fault zones. The Maoping deposit mainly consists of three ore bodies (groups), of which the No. I ore body (group) is hosted in the Upper Devonian Zhaige Formation dolostone, the No. II ore body (group) is hosted in the Lower Carboniferous Baizuo Formation dolostone, and the No. III ore body (group) is hosted by dolostone of the Upper Carboniferous Weining Formation. The ores are mainly composed of ore minerals, such as sphalerite, galena and pyrite, and gangue minerals, for example, dolomite and calcite with a small amount of quartz and barite. Those hydrothermal minerals have massive, disseminated or veined structures, and have granular, metasomatic, co-edge, colloidal, aggregate or fragmentation textures. Hence, the epigenetic ore-forming characteristics of the Maoping deposit are obvious. The Nano-SIMS in-situ S isotopic compositions show that the fine-grained strawberry aggregate pyrite and colloidal sphalerite had a significant depletion of ^{34}S , and their $\delta^{34}\text{S}$ values range from -20.4‰ to -8.7‰. Such sulfur isotope signatures have typical biogenetic sulfur characteristics, suggesting that they had undergone marine sulfate bacterial reduction process (BSR). On the other hand, the in-situ $\delta^{34}\text{S}$ values of granular pyrite and sphalerite vary from 22.1‰ to 25.6‰, obviously enriched in heavy sulfur isotopes, indicating that they had undergone a marine sulfate thermochemical reduction process (TSR). Since BSR and TSR are mainly temperature dependent, the formation of S^{2-} in the Maoping deposit was local reduced and may first undergo a relatively low temperature BSR process, and then undergo a relatively high temperature TSR process. The fs LA-MC-ICPMS in-situ Pb isotopic ratios of galena show that Pb isotopic ratios of galena are relatively uniform, suggesting that the source of Pb is single or well-mixed. The comparison indicates that the ore-forming metals of the Maoping deposit were mainly derived from ore-bearing sedimentary rocks with a certain influence of underlying basement rocks. In addition, the in-situ Pb isotopic ratios of galena have a tendency to increase with the increase of the elevation, suggesting that the migration direction of the ore-forming fluid is most likely upward, and with the evolution of ore-forming fluids, the radiogenic Pb-rich sedimentary rocks contributed more ore-forming metals. Hence, this paper considers that the Maoping large-scale Pb-Zn deposit is the product of fluid

* 本文受国家重点研发计划项目(2017YFC0602502)、国家自然科学基金项目(41430315、41872095)、云南大学引进人才科研启动项目(YJRC4201804)和云南大学国家杰出(优秀)青年培育项目(2018YDJQ009)联合资助。

第一作者简介: 谈树成, 男, 1970年生, 博士, 教授, 主要从事矿床学研究和教学工作, E-mail: 695602890@qq.com

** 通讯作者: 周家喜, 男, 1982年生, 博士, 研究员, 主要从事低温热液矿床成因研究, E-mail: zhoujiaxi@ynu.edu.cn

mixing and its deep may have a good prospecting potential, as the metal-rich basements contribute more in deep.

Key words NanoSIMS in-situ S isotopes; LA-MC-ICPMS in-situ Pb isotopes; The sources of ore-forming elements; Ore formation processes; Ore prospecting direction; The Maoping large-scale Pb-Zn deposit

摘要 位于扬子板块西缘的川滇黔铅锌集区是我国重要的贱金属生产基地之一。矿集区中部的毛坪大型铅锌矿床,累计探明铅锌金属储量超过300万吨,Pb+Zn平均品位12%~30%,局部达45%,是矿集区内第二大铅锌矿床。矿体呈似层状、透镜状或脉状集中分布于猫猫山背斜NW倒转翼及其倾伏端NE向层间断裂带内。主要发育3个矿体(群),其中I号矿体(群)赋存于上泥盆统宰格组白云岩中,II号矿体(群)赋存于下石炭统摆佐组白云岩中,III号矿体(群)赋存于上石炭统威宁组白云岩中。矿石主要由闪锌矿、方铅矿和黄铁矿等矿石矿物及白云石和方解石(少量石英和重晶石)等脉石矿物组成,具有块状、浸染状或脉状构造及粒状、交代、共边、胶状、集合体或碎裂结构。可见,该矿床后生成矿特征明显。纳米离子探针(NanoSIMS)原位S同位素组成分析结果显示,细粒草莓集合体状黄铁矿和胶状闪锌矿明显亏损³⁴S,其δ³⁴S值变化范围为-20.4‰~ -8.7‰之间,具有典型生物成因S特征,暗示经历了海相硫酸盐细菌还原过程(BSR);而自形粒状黄铁矿和他形粒状闪锌矿的δ³⁴S值变化范围为22.1‰~ 25.6‰之间,明显富集重S同位素,表明经历了海相硫酸盐热化学还原过程(TSR)。由于BSR和TSR过程主要受温度控制,因此,还原态硫离子的形成最可能是原地还原的,并先经历了相对低温的BSR过程,再经历了相对高温的TSR过程。飞秒激光剥蚀多接收器等离子体质谱(fs LA-MC-ICPMS)原位Pb同位素组成分析结果显示,方铅矿的Pb同位素组成相当均一,暗示其来源单一或混合均匀,对比显示其成矿金属主要由赋矿沉积岩提供,受到一定程度的下伏基底岩石影响。此外,方铅矿的原位Pb同位素组成有随着标高增加而升高的趋势,暗示成矿流体的运移方向很可能是向上的,且随着成矿流体的演化,富放射性成因Pb的赋矿沉积岩贡献了更多的成矿金属。综上,本文认为毛坪大型铅锌矿床是流体混合作用的产物,其深部可能具有良好找矿潜力,这是因为富含金属元素的基底岩石对深部贡献更多。

关键词 NanoSIMS 原位S同位素; LA-MC-ICPMS 原位Pb同位素; 成矿物质来源; 成矿过程; 找矿方向; 毛坪大型铅锌矿床

中图法分类号 P611. 1; P597. 2; P628. 42; P618. 43

位于扬子板块西缘四川、云南和贵州三省接壤区约17万平方千米的范围内,发育铅锌矿床(点)500余处(柳贺昌和林文达,1999统计为400余处),构成著名的川滇黔铅锌矿集区(王奖臻等,2002;张长青等,2005; Zhou et al., 2013a)。该区是华南大面积低温成矿域的重要组成部分之一(黄智龙等,2011;胡瑞忠等,2016; Hu et al., 2017a; Zhou et al., 2018a),也是我国重要的铅、锌、银、锗等资源基地之一(黄智龙等,2004; Zhou et al., 2013b; Zhang et al., 2015)。区内的铅锌矿床主要赋存于新元古界至中二叠统碳酸盐岩中,受断层褶皱构造体系控制明显,前人对其属于后生热液成因的认识基本趋于一致,但对它们是否属于MVT矿床还存有争议(黄智龙等,2001;刘家铎等,2003;李文博等,2004; Wu et al., 2013; Xu et al., 2014; Zhou et al., 2014a, 2015, 2018b; 金中国等,2016; 梁峰等,2016; 孙海瑞等,2016; 崔银亮等,2018)。毛坪铅锌矿床累计探明铅锌金属储量超过300万吨,是川滇黔铅锌矿集区内已知除会泽超大型铅锌矿床(探明铅锌金属储量超过500万吨)之外规模最大的铅锌矿床(韩润生等,2010),但毛坪矿床的研究远不及会泽矿床的程度高。虽然毛坪与会泽两个矿床间有诸多相似之处,但它们间也有很多不同之处。例如,毛坪矿床赋存于上泥盆统宰格组、下石炭统摆佐组和上石炭统威宁组三个层位中(邹海俊等,2004; 韩润生等, 2007; Wei et al., 2015),而会泽矿床则赋存于下石炭统摆佐组中(黄智龙等,2004; 李文博等, 2004, 2006; Huang et al., 2010)。因此,开展毛坪大型铅锌矿床的深入研究和比较矿床学分析,不仅能为理解其成因机制提供重要参考信息,也对指导研究

区多层次找矿具有重要现实意义。

越来越多的研究表明,流体混合是诸多热液矿床形成的重要机制(华仁民,1994; 魏文凤等,2011; Zhou et al., 2013c, 2014b, 2016a; 金若时等,2014),而在以碳酸盐岩为容矿围岩的后生热液铅锌矿床的形成中,流体混合可能也是导致海相硫酸盐热化学还原(TSR)、水/岩相互作用(W/R)和CO₂去气等过程发生的重要因素(Zhou et al., 2018c)。尽管前人对包括毛坪铅锌矿床在内的整个川滇黔铅锌矿集区硫主要来源于赋矿地层中富含石膏等海相硫酸盐的蒸发膏盐层、金属主要来源于赋矿沉积岩和下伏基底岩石、流体混合是导致金属硫化物沉淀主要机制的认识已基本达成共识(张长青等,2005; Zhou et al., 2013d, 2015; 金中国等,2016; Liu et al., 2017; 陈伟等,2017; Kong et al., 2018; 崔银亮等,2018; 任顺利等,2018),但对蒸发膏盐层中海相硫酸盐的还原,是发生在流体混合前还是流体混合后,有不同认识(Zhou et al., 2013e; 秦建华等,2016; Liu et al., 2017; 杨兴玉等,2018)。S和Pb是铅锌硫化物矿床的两个主要成矿元素,其同位素组成能有效约束自身的来源、形成机制和演化过程等,已被广泛应用于此类矿床成因和形成过程研究中(李文博等,2006; Zhou et al., 2010, 2016b; 周家喜等,2010, 2012; Li et al., 2015, 2016; Tan et al., 2017, 2019; Zhu et al., 2016, 2017; Wang et al., 2018; 安琦等,2018)。虽然以碳酸盐岩为容矿围岩的后生热液铅锌矿床,其矿物组合相对简单(主要为硫化物+碳酸盐矿物),但各矿物间的共边、包裹、穿插和交代等现象非常普遍,分选出100%纯净单矿物的可能性很小,所以传统方法获得硫化物单矿物S和Pb

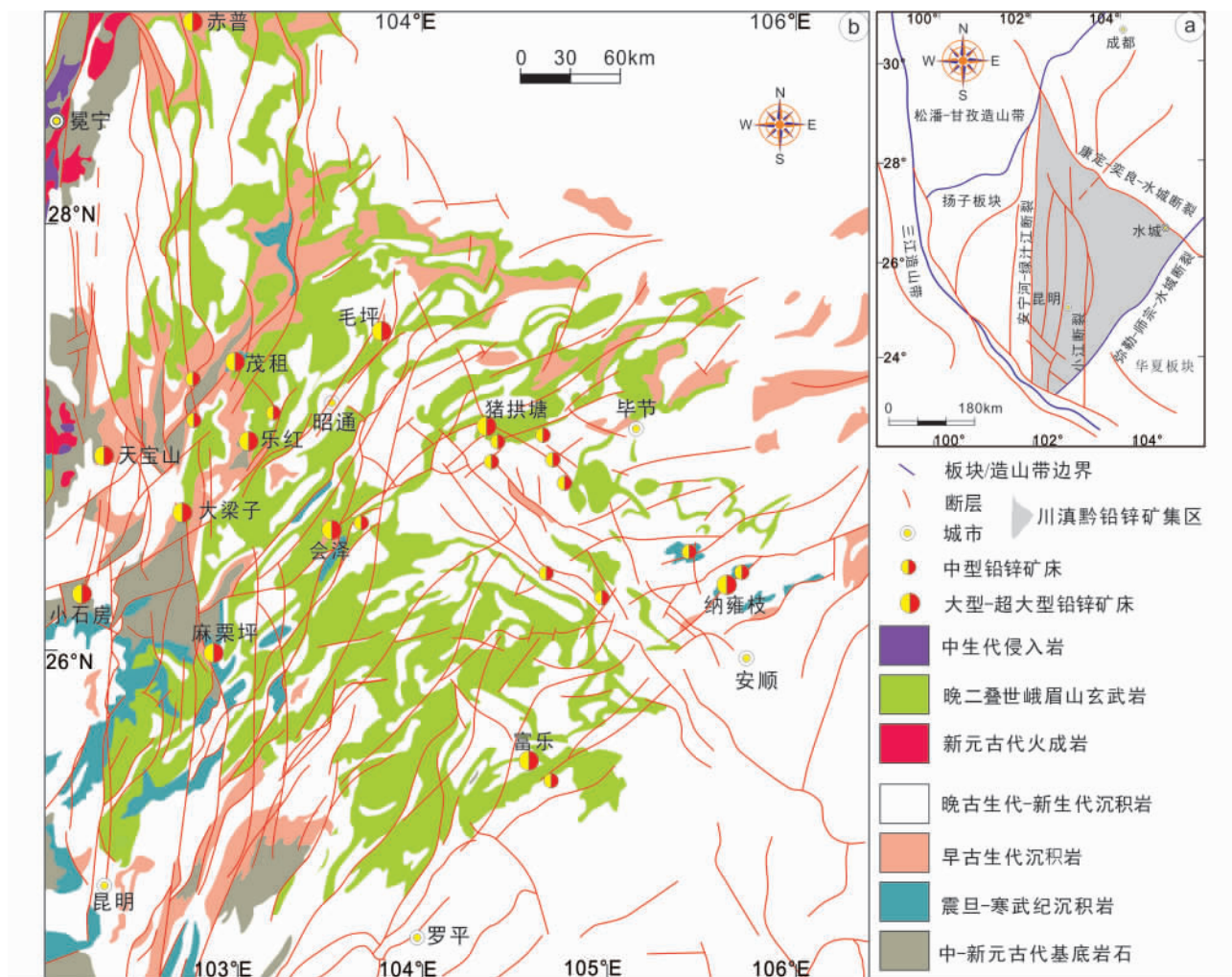


图 1 扬子板块西缘构造背景(a) 及川滇黔铅锌矿集区地质略图(b)(据 Zhou et al. , 2018a 修改)

Fig. 1 The tectonic setting of the western Yangtze Block (a) and the sketch geological map of the Sichuan-Yunnan-Guizhou Pb-Zn metallogenic province (b) (modified after Zhou et al. , 2018a)

等同位素组成很可能是混合值,从而掩盖了一些可能非常重要的成矿信息(Zhang et al. , 2014; Bao et al. , 2016, 2017; 金中国等, 2016; Wang et al. , 2018; Zhou et al. , 2018a, b; Luo et al. , 2019a, b)。本文借助纳米离子探针(NanoSIMS)和飞秒激光剥蚀多接收器等离子体质谱(fs LA-MC-ICPMS),对采自毛坪大型铅锌矿床不同矿体及其不同中段矿石样品中主要硫化物(黄铁矿、闪锌矿和方铅矿),开展原位 S 和 Pb 同位素地球化学研究,旨在查明该矿床的成矿物质来源、还原态硫离子的形成机制和成矿的精细过程,为理解此类矿床成因和指导找矿预测提供新信息。

1 区域地质背景

川滇黔铅锌矿集区处于扬子板块西缘(图 1a),属于全球特提斯成矿域与环太平洋成矿域的交汇部位,在空间上位于峨眉山大火成岩省内(图 1b),是我国以碳酸盐岩为容矿

围岩的后生热液铅锌矿床最为集中发育的地区(王奖臻等, 2001; 范宗瑶等, 2004; 黄智龙等, 2011; 毛景文等, 2012; 张长青等, 2013; Hu et al. , 2017a; Zhou et al. , 2018a)。扬子地块西缘基底具有“双层结构”,即由太古代(如 3.3 ~ 2.9Ga 的崆岭杂岩)-古元古代结晶基底(如 2.45 ~ 2.06Ga 的康定群)和中-新元古代褶皱基底(如 1.7Ga 的东川群和 1.1Ga 的会理/昆阳群)组成(Qiu et al. , 2000, 2016; Zhao et al. , 2010; Gao et al. , 2011; Zhou et al. , 2015) ,而盖层则具有“三层结构”,即由古生代至早中生代海相沉积岩、晚二叠世峨眉山大陆溢流玄武岩和晚中生代至新生代陆相沉积岩组成(柳贺昌和林文达, 1999; Zhou et al. , 2002; 黄智龙等, 2004)。其中中-新元古界至中二叠统碳酸盐岩是研究区铅锌矿床的赋矿围岩,而赋矿地层中富含石膏等海相硫酸盐的蒸发膏盐层和有机质则被认为是这些铅锌矿床的主要硫源和还原剂(Zhou et al. , 2013e, 2018a; Liu et al. , 2017; Kong et al. , 2018)。二叠纪以来,扬子地块西缘经历的主要构造-

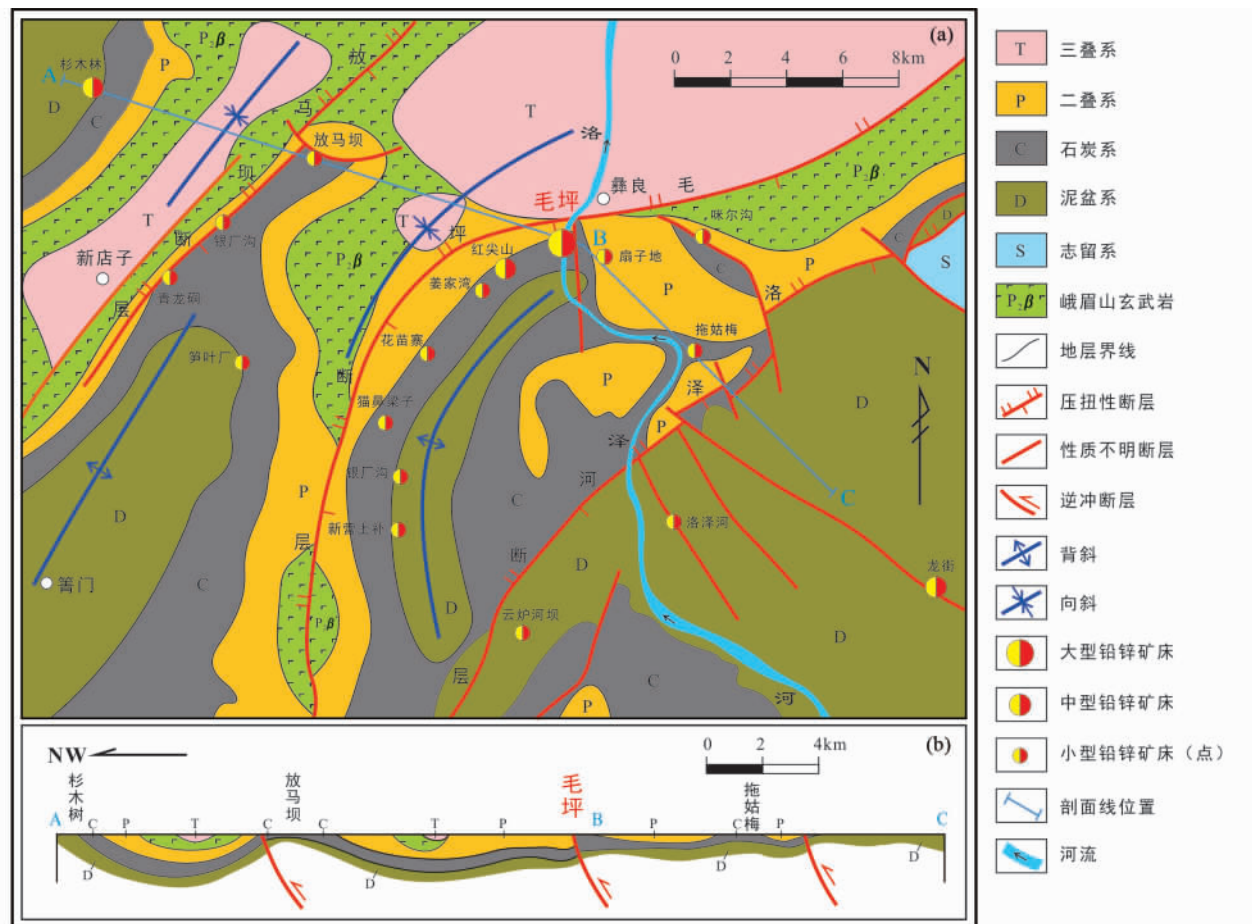


图2 毛坪地区地质略图(a) 及剖面图(b) (据韩润生等, 2012 修改)

Fig. 2 The sketch geological map (a) and the profile section map (b) of the Maoping area (modified after Han et al. , 2012)

热事件有海西、印支、燕山和喜山运动及峨眉山地幔柱，其中晚二叠世峨眉山地幔柱形成的大火成岩省最具特色(Zhou et al. , 2002) ,其溢流玄武岩的分布范围在空间上与研究区铅锌矿床叠置(图 1b) 。除少量砂矿(铅锌氧化矿) 外,川滇黔铅锌矿集区内全部铅锌矿床均赋存于峨眉山玄武岩之下的各时代地层碳酸盐岩中,暗示这些铅锌矿床的形成时代要晚于~260Ma 的峨眉山地幔柱(Zhou et al. , 2002; 黄智龙等, 2001) 。研究区的构造主要发育近 NS、NE 和 NW 向三组,这些构造具有多期活动的特征,并显著控制区内铅锌矿床的分布(图 1b) 。与铅锌成矿有关的构造变形应力、应变场分析显示,与区域变形相对应的区域性应力场有印支晚期和燕山期两期(张志斌等, 2006) 。硫化物 Rb-Sr 和含钙矿物(方解石和萤石) Sm-Nd 同位素年代学研究显示,本区铅锌矿床很可能形成于 230 ~ 200Ma(李文博等, 2004; 蔺志永等, 2010; 毛景文等, 2012; Zhou et al. , 2013a, b, 2015; Zhang et al. , 2015) 。

2 矿床地质特征

毛坪地区出露的地层以古生界为主(图 2) ,地层从老到

新依次为志留系、泥盆系、石炭系、二叠系和三叠系。中志留统至中泥盆统岩性以浅海相碎屑岩夹碳酸盐岩为主,上泥盆统至下二叠统岩性以浅海相碳酸盐岩夹少量滨海相碎屑岩为主,而上二叠统则是陆相玄武岩及海陆交互相含煤建造,中-下三叠统主要为浅海相碎屑岩夹碳酸盐岩,上三叠统则是含煤建造和河湖相红色建造(沈战武等, 2016) 。毛坪矿区出露的地层主要为上泥盆统宰格组、下石炭统大塘组和摆佐组、上石炭统威宁组、下二叠统梁山组、中二叠统栖霞-茅口组和上二叠统峨眉山玄武岩组。有关这些地层单元主要的岩性,请参阅相关文献(邹海俊等, 2004; 韩润生等, 2007; 申屠良义等, 2011; 魏爱英等, 2012) ,在此不再赘述。

毛坪铅锌矿区位于区域性昭通-曲靖隐伏断裂和垭都-紫云深大断裂的复合部位,构造形迹以 NE 和 NW 向为主,主干构造包括石门坎背斜以及毛坪和洛泽河断层等(图 2a) 。在石门坎背斜的 NW 翼深部,还发育有 NW-SE 向挤压应力形成的层间断裂和剥离构造带,表现出强烈层间挤压滑动性质(魏爱英等, 2012) 。研究区除晚二叠世峨眉山玄武岩广泛分布外,其它类型岩浆岩不发育(图 2) 。

毛坪铅锌矿床主要发育 3 个矿体(群) ,均呈似层状、透

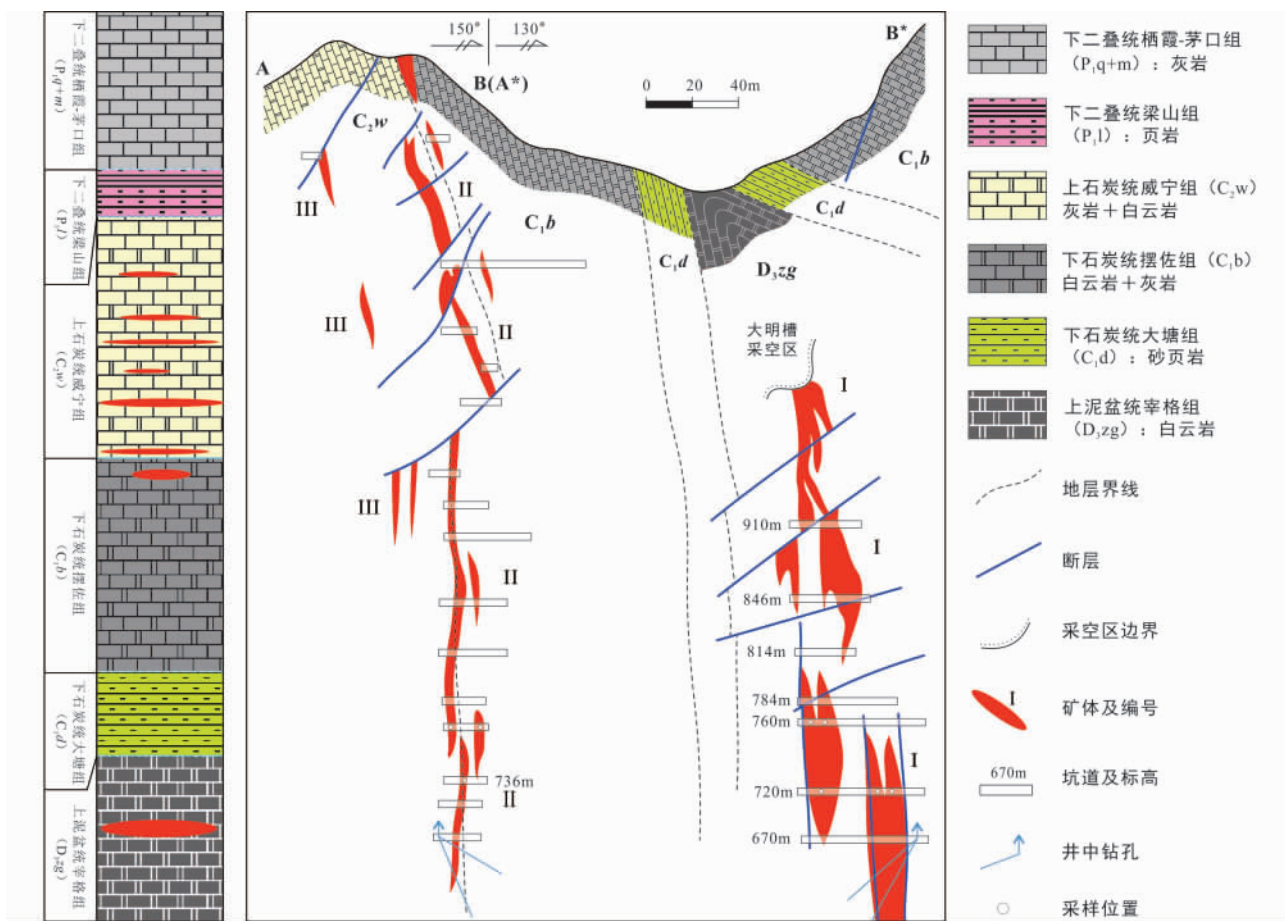


图3 毛坪铅锌矿床典型剖面综合图(据 Wei et al., 2015 修改)

Fig. 3 The typical profile comprehensive map (modified after Wei et al., 2015)

镜状或脉状集中分布于猫猫山背斜 NW 倒转翼及其倾伏端 NE 向层间断裂带内(图 2、图 3), 其中 I 号矿体(群)的赋矿围岩为上泥盆统宰格组白云岩, II 号矿体(群)赋存于下石炭统摆佐组白云岩中, III 号矿体(群)的赋矿围岩为上石炭统威宁组白云岩(图 3)。毛坪矿区 I 号矿体规模最大, 所以本文以 I 号矿体为例介绍矿体特征, 该矿体走向 NE-SW, 与地层走向一致, 长为 280~320m, 倾向 SE, 倾角 70°~85°, 倾斜延伸大于 370m(地表露头标高 1040m, 坑道控制深度标高 670m), 水平厚度 5.21~30.4m, 平均厚 17.93m。矿体的 Zn 品位为 3.9%~30.94%, 平均品位为 12.81%, Pb 品位为 2.64%~13.09%, 平均品位为 5.46%。

毛坪矿区矿石矿物以闪锌矿、方铅矿和黄铁矿为主(图 4a-o), 含少量白铁矿、毒砂和黄铜矿, 脉石矿物主要为白云石和方解石, 含少量的石英、重晶石和沥青(韩润生等, 2007)。矿石的主要构造有致密块状、稠密浸染状、条带状、细脉状和网脉状(图 4a-f)。金属硫化物矿物和碳酸盐矿物(白云石/方解石)具有粒状、交代、共边、胶状、集合体和碎裂等结构(图 4g-o)。根据魏爱英等(2012)的研究, 毛坪铅锌矿床不同构造的矿石具有一定的分带特征, 即致密块状矿石位于矿体中部, 向外依次为稠密浸染状、脉状和稀疏浸染星点

状。根据矿石组构特征, 将毛坪铅锌矿床成矿期分为三个主要阶段: 即黄铁矿-闪锌矿-石英±白云石阶段、闪锌矿-方铅矿-黄铁矿-白云石/方解石阶段和白云石/方解石±重晶石阶段。矿区围岩蚀变主要有硅化和碳酸盐化, 具有一定的分带性, 从内到外依次为硅化、铁白云石化、白云石化和方解石化(魏爱英等, 2012; Wei et al., 2015)。

3 样品来源和分析方法

3.1 样品来源

本次研究采集的 80 余件样品来自毛坪铅锌矿床的 I 和 II 号矿体(群)的 760m、736m 和 720m 中段(采样位置如图 3 所示), 包括块状、脉状和浸染状矿石(图 4a-f)。样品经详细的宏观观测、描述和拍照后, 进行光薄片磨制, 在显微镜和扫描电镜详细的矿物学观察后, 选择不同结构的黄铁矿、闪锌矿和方铅矿等硫化物颗粒位置, 以备原位 S 和 Pb 同位素组成分析。由于 2015 年底开展此项研究时, NanoSIMS 原位 S 同位素组成分析缺乏方铅矿标样, 而 fs LA-MC-ICPMS 原位 Pb 同位素组成分析无法扣除闪锌矿和黄铁矿中²⁰⁴Hg 对²⁰⁴Pb 的影响, 因此本研究仅对 I 号矿体的闪锌矿和方铅矿进行原位 S 和 Pb 同位素组成分析。

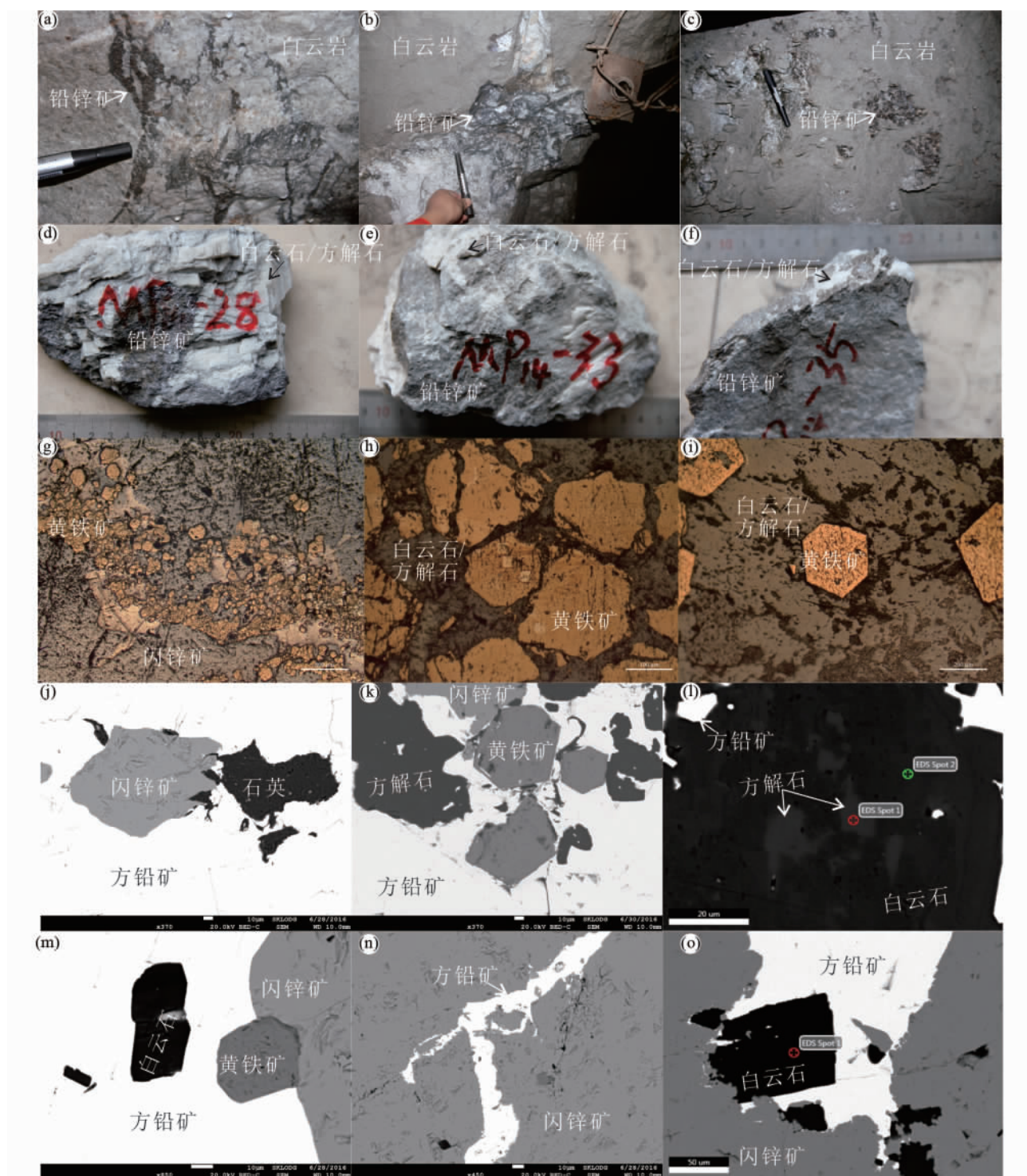


图4 毛坪铅锌矿床矿体、矿石和矿物特征

(a-c) 毛坪铅锌矿床矿体典型宏观特征; (d-f) 矿石手标本典型宏观特征; (g-i) 矿物显微镜下典型微观特征; (j-o) 矿物扫描电镜下典型微观特征

Fig. 4 The features of ore bodies, ores and minerals for the Maoping Pb-Zn deposit

(a-c) the typical macroscopic features of ore bodies in the Maoping deposit; (d-f) the typical macroscopic features of ore hand specimens; (g-i) the typical microscopic features of minerals under microscope; (j-o) the typical microscopic features of minerals under SEM

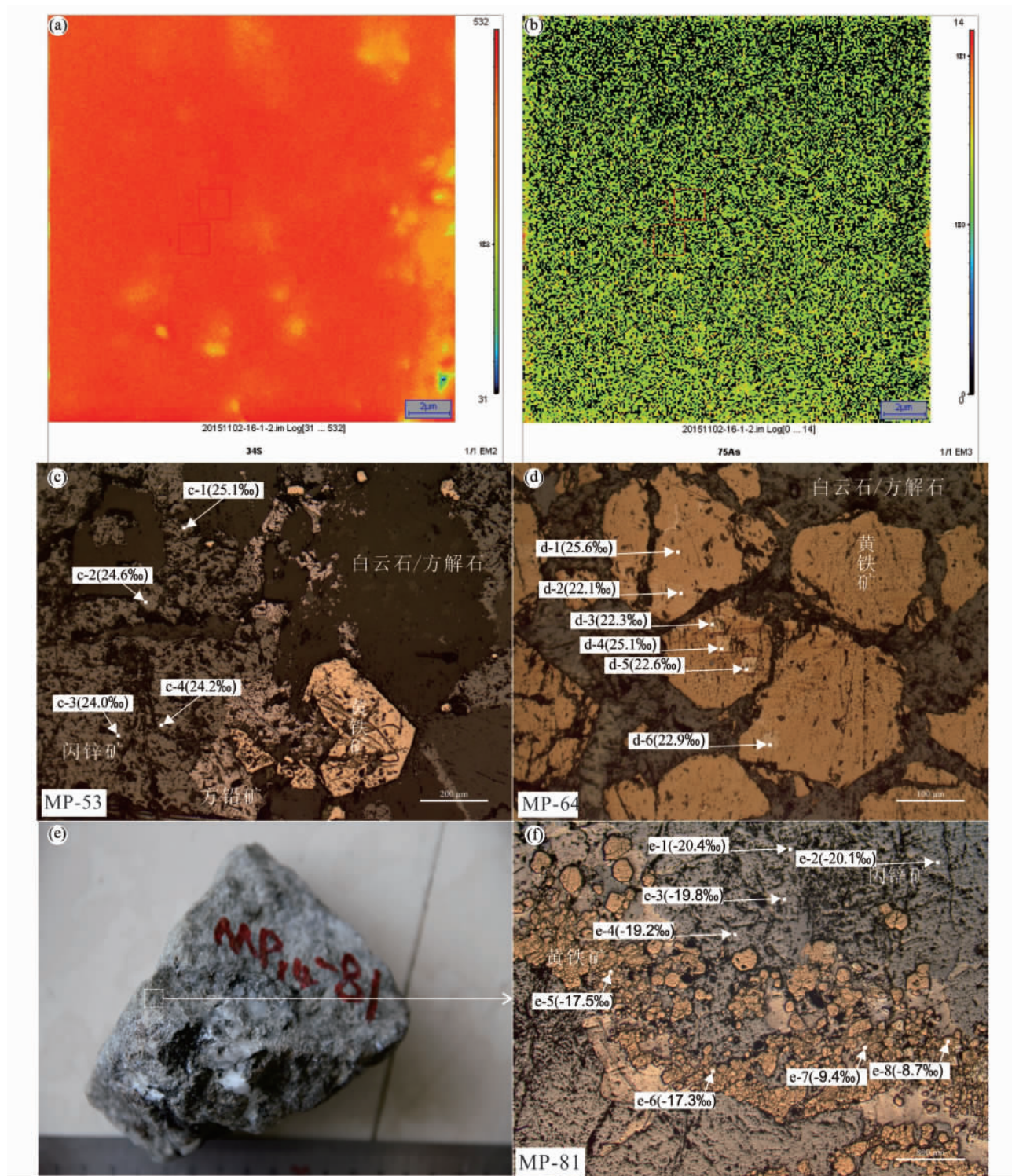


图 5 毛坪铅锌矿床原位 S 同位素分析测点特征

(a, b) 毛坪铅锌矿床原位 S 同位素测点元素 Mapping; (c, d, f) 黄铁矿和闪锌矿原位 S 同位素组成; (e) 原位 S 同位素测试手标本

Fig. 5 The features of in-situ S isotope analysis points for the Maoping Pb-Zn deposit

(a, b) in-situ S isotope testing element mapping of the Maoping Pb-Zn deposit; (c, d, f) in-situ S isotopic compositions of pyrite and sphalerite; (e) in-situ S isotope testing hand specimen

的影响,所以原位 S 和 Pb 同位素组成分析未能同样品、同位置配套开展。

3.2 NanoSIMS 原位 S 同位素组成分析

黄铁矿和闪锌矿的原位 S 同位素组成分析是在中国科学院地质与地球物理研究所的纳米离子探针(NanoSIMS) 实验室完成,分析所用的仪器型号为 CAMECA NanoSIMS 50L。该仪器通过小至 50nm 的 Cs^+ 离子束扫描硫化物颗粒表面,能同时获得多个同位素的高分辨率图像。为满足空间分辨率不同的需求,该仪器配备有多个法拉第杯和/或电子倍增器(FC-EM)。实验分析过程采用标样-样品-标样交叉分析模式,确保数据精确可靠。为了减少矿物晶体不同部位元素组成变化对 S 同位素分馏产生影响,分析点尽量选择同位素分布均匀区域(图 5a, b)。采用的标样有国际标样 CAR 123 (黄铁矿) 和 Balmat(黄铁矿和闪锌矿) 以及内部标样 CS 01 (黄铁矿) 、PY 1117(黄铁矿) 、MY 09-42(闪锌矿) 和 JC 14 (闪锌矿)。对未知样品的重复分析 S 同位素组成误差优于 0.2‰(1σ) ,该仪器详细参数和实验流程见相应文献(Zhang et al. , 2014; 杨兴玉等, 2018; Zhou et al. , 2018a)。

3.3 LA-MC-ICPMS 原位 Pb 同位素组成分析

方铅矿 fs LA-MC-ICPMS 原位 Pb 同位素组成分析在西北大学大陆动力学国家重点实验室完成。分别用 2% HNO_3 和超纯水超声清洗整个样品靶(光薄片) 以尽可能去除样品表明的污染物,并以高纯 Ar 或 N_2 气枪吹干,待测。仪器型号为 Nu Instruments 公司的 Nu Plasma II 型 MC-ICPMS,激光器型号为 Quantronix Integra-HE Ti 266 nm NWR UP Femto (ESI, USA) ,剥蚀半径为 15~65 μm ,激光频率 5~50Hz,剥蚀方式为 3 $\mu\text{m}/\text{s}$ 线扫描,He 气流为 0.7L/min。采用标样-样品-标样交叉法,标样为 NIST 610,分析误差优于 0.003(1σ) ,详细仪器参数和实验流程见相应文献(Yuan et al. , 2015, 2016; Bao et al. , 2016, 2017; 金中国等, 2016; Zhou et al. , 2018b; 安琦等, 2018)。

4 结果

4.1 原位 S 同位素组成

黄铁矿和闪锌矿的 NanoSIMS 原位 S 同位素组成分析结果列于表 1 和图 5c, d, f。可见全部黄铁矿和闪锌矿原位 $\delta^{34}\text{S}$ 值变化范围为 $-20.4\text{\textperthousand} \sim 25.6\text{\textperthousand}$ 之间,可分为两组:即细粒草莓集合体状黄铁矿和胶状闪锌矿的 $\delta^{34}\text{S}$ 值变化范围为 $-20.4\text{\textperthousand} \sim -8.7\text{\textperthousand}$ 之间,明显亏损 ^{34}S ;而自形粒状黄铁矿和他形粒状闪锌矿的 $\delta^{34}\text{S}$ 值变化范围为 $22.1\text{\textperthousand} \sim 25.6\text{\textperthousand}$ 之间,则明显富集重 S 同位素。此外,自形粒状黄铁矿颗粒不同部位的 $\delta^{34}\text{S}$ 值也有所不同(图 5d) ,例如样品 MP-64 中黄铁矿边部的 $\delta^{34}\text{S}$ 值($22.1\text{\textperthousand} \sim 22.9\text{\textperthousand}$) 要略低于其中部 ($25.1\text{\textperthousand} \sim$

表 1 毛坪铅锌矿床闪锌矿和黄铁矿原位 S 同位素组成

Table 1 In-situ S isotopic compositions of sphalerite and pyrite from the Maoping deposit

样品号	测点号	产状	$\delta^{34}\text{S}$ (‰)
MP-53	c-1	他形粒状闪锌矿中部	25.1
	c-2	他形粒状闪锌矿中部	24.6
	c-3	他形粒状闪锌矿中部	24.0
	c-4	他形粒状闪锌矿中部	24.2
MP-64	d-1	自形粒状黄铁矿中部	25.6
	d-2	自形粒状黄铁矿边部	22.1
	d-3	自形粒状黄铁矿边部	22.3
	d-4	自形粒状黄铁矿中部	25.1
	d-5	自形粒状黄铁矿边部	22.6
	d-6	自形粒状黄铁矿边部	22.9
MP-81	e-1	细粒集合体草莓状黄铁矿中部	-17.5
	e-2	细粒集合体草莓状黄铁矿中部	-17.3
	e-3	细粒集合体草莓状黄铁矿中部	-9.4
	e-4	细粒集合体草莓状黄铁矿中部	-8.7
	e-5	胶状闪锌矿中部	-20.4
	e-6	胶状闪锌矿中部	-20.1
	e-7	胶状闪锌矿中部	-19.8
	e-8	胶状闪锌矿中部	-19.2

25.6‰)。

4.2 原位 Pb 同位素组成

方铅矿的 LA-MC-ICPMS 原位 Pb 同位素组成分析结果列于表 2。可见毛坪铅锌矿床方铅矿的 18 个测点 Pb 同位素组成比较集中,其 $^{206}\text{Pb}/^{204}\text{Pb}$ 、 $^{207}\text{Pb}/^{204}\text{Pb}$ 和 $^{208}\text{Pb}/^{204}\text{Pb}$ 比值分别为 $18.712 \sim 18.768$ (均值为 18.739) , $15.786 \sim 15.796$ (均值为 15.791) 和 $39.399 \sim 39.513$ (均值为 39.452) 。

5 讨论

5.1 还原态硫离子的来源、形成过程和分馏机制

5.1.1 还原态硫离子的来源

申屠良义等(2011) 采用传统方法对毛坪铅锌矿床进行了较为系统和全面的 S 同位素地球化学研究,结果显示该矿床硫化物的 $\delta^{34}\text{S}$ 值为 $7\text{\textperthousand} \sim 24\text{\textperthousand}$,据此其认为毛坪矿床的还原态硫离子来源于赋矿地层中富含石膏等海相硫酸盐的蒸发膏盐层。为了进一步弄清矿石硫化物中的还原态硫离子是否源自海相蒸发膏盐层,任顺利等(2018) 对毛坪矿床赋存于不同层位中的矿石硫化物和膏盐层中的石膏,进行了全面和深入的 S 同位素组成分析和对比研究,结果显示赋存于宰格组白云岩中的矿石硫化物,其 $\delta^{34}\text{S}$ 值为 $18.3\text{\textperthousand} \sim 22.7\text{\textperthousand}$ (均值为 $21.1\text{\textperthousand}$),与之对应的泥盆系膏盐层中的石膏,其 $\delta^{34}\text{S}$ 值为 $21.9\text{\textperthousand} \sim 25.9\text{\textperthousand}$ (均值为 $23.6\text{\textperthousand}$) ,二者几乎完全一致;赋存于摆佐组白云岩中的矿石硫化物,其 $\delta^{34}\text{S}$ 值为 $7\text{\textperthousand} \sim 17.5\text{\textperthousand}$ (均值为 $12.8\text{\textperthousand}$) ,与之对应的石炭系膏盐层中的

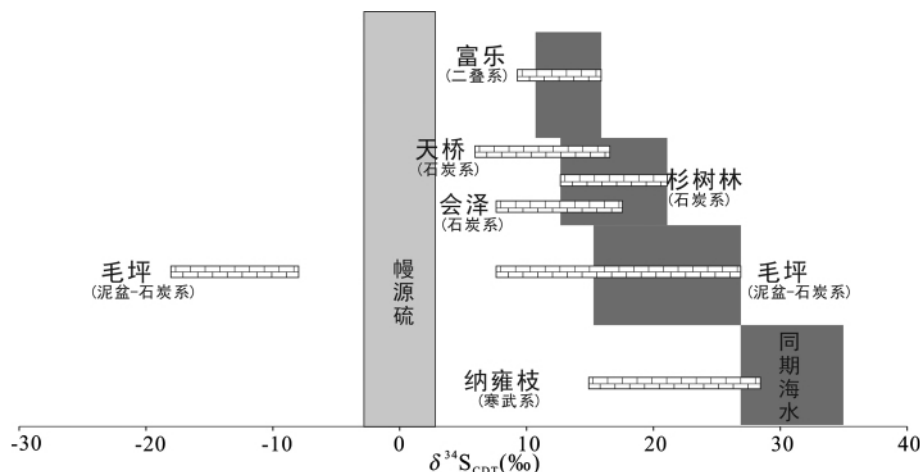


图 6 川滇黔铅锌矿集区不同时代地层中铅锌矿床与同期海水和幔源硫的硫同位素组成对比

数据来源: 幔源硫同位素组成范围据 Chaussidon *et al.* (1989), 同期海水硫同位素组成范围据 Claypool *et al.* (1980), 矿床硫同位素来自文献 (李文博等, 2006; Zhou *et al.*, 2013a, 2014b; 金中国等, 2016; 崔银亮等, 2018; 任顺利等, 2018; 任涛等, 2019)

Fig. 6 Comparison of S isotopic compositions between the Pb-Zn deposits hosted in different strata ages of the Sichuan-Yunnan-Guizhou Pb-Zn metallogenic province and the seawater and mantle-derived sulfur

Data sources: mantle-derived sulfur are from Chaussidon *et al.* (1989); seawater sulfur are from Claypool *et al.* (1980); and ore deposit sulfur are from Li *et al.* (2006), Zhou *et al.* (2013a, 2014b), Jin *et al.* (2016), Cui *et al.* (2018) and Ren *et al.* (2018, 2019)

石膏, 其 $\delta^{34}\text{S}$ 值为 $12.9\text{\textperthousand} \sim 17.1\text{\textperthousand}$ (均值为 $13.6\text{\textperthousand}$), 二者也颇为相似。本次分析获得的矿石硫化物的原位 $\delta^{34}\text{S}$ 值可分为 $-20.4\text{\textperthousand} \sim -8.7\text{\textperthousand}$ 和 $22.1\text{\textperthousand} \sim 25.6\text{\textperthousand}$ 两组(表 1), 可见后者完全落入传统方法报道的矿石硫化物的 $\delta^{34}\text{S}$ 值结果范围内($7\text{\textperthousand} \sim 26\text{\textperthousand}$: 申屠良义等, 2011; 任顺利等, 2018), 表明毛坪铅锌矿床还原态硫离子确实来自赋矿地层中富含石膏等海相硫酸盐的蒸发膏盐层。区域上, 包括纳雍枝(赋存于寒武系; 金中国等, 2016; Zhou *et al.*, 2018c)、会泽(赋存于石炭系; 李文博等, 2006; 任顺利等, 2018)、杉树林(赋存于石炭系; Zhou *et al.*, 2014b)、天桥(主要赋存于石炭系; Zhou *et al.*, 2013a; Liu *et al.*, 2017) 和富乐(赋存于二叠系; Zhou *et al.*, 2018b; 崔银亮等, 2018; 任涛等, 2019) 等铅锌矿床(图 6), 其还原态硫离子也是来自赋矿地层中的海相蒸发膏盐层(Zhou *et al.*, 2013e), 这与全球 MVT 矿床中还原态硫离子主要来自海水硫酸盐的认识是一致的(Leach *et al.*, 2005, 2010)。综上, 赋矿地层中的海相蒸发膏盐层不仅是研究区铅锌矿床的主要硫源, 而且还可以作为本区铅锌矿床定位预测的重要找矿标志。

5.1.2 还原态硫离子的形成过程和分馏机制

海相硫酸盐的还原主要通过无机的热化学还原(TSR)和有机的细菌还原(BSR) (Ohmoto, 1972, 1986; Seal, 2006)两个过程。TSR 和 BSR 过程均是温度依赖的, 即 TSR 过程需要达到启动热化学反应的温度条件, 主要发生在相对较高的温度条件下($> 100 \sim 120^\circ\text{C}$; Ohmoto, 1972; Claypool *et al.*, 1980; Seal, 2006), 而 BSR 过程需要满足还原细菌存活的温度条件, 通常发生在相对低温($< 100 \sim 120^\circ\text{C}$; Jørgenson *et al.*, 1992; Basuki *et al.*, 2008)的条件下。此外, TSR 过程

能快速产生大量 S^{2-} , 且其 $\delta^{34}\text{S}$ 值相对集中、变化范围较小, 与 SO_4^{2-} 的 $\delta^{34}\text{S}$ 值差, 即 $\Delta^{34}\text{S}(\text{SO}_4^{2-}-\text{S}^{2-})$ 可达 $15\text{\textperthousand} \sim 20\text{\textperthousand}$; 而 BSR 过程形成 S^{2-} 需要较长时间, 且形成 S^{2-} 的 $\delta^{34}\text{S}$ 值明显偏负、变化范围也较宽, 与 SO_4^{2-} 的 $\delta^{34}\text{S}$ 值差, 即 $\Delta^{34}\text{S}(\text{SO}_4^{2-}-\text{S}^{2-})$ 高达 $40\text{\textperthousand}$ (Ohmoto, 1986; Ohmoto and Goldhaber, 1997; Basuki *et al.*, 2008)。前人(申屠良义等, 2011; 任顺利等, 2018)认为 TSR 过程是毛坪矿床 S^{2-} 形成的主要机制, 因为毛坪矿床的成矿温度($180 \sim 218^\circ\text{C}$; 韩润生等, 2007) 明显高于细菌存活的温度($< 100 \sim 120^\circ\text{C}$; Jørgenson *et al.*, 1992; Basuki *et al.*, 2008), 且毛坪矿床矿石硫化物具有明显富集重 S 同位素特征($7\text{\textperthousand} \sim 26\text{\textperthousand}$: 申屠良义等, 2011; 任顺利等, 2018)。但是, 本次研究发现毛坪矿床除富集重 S 同位素(图 5c, d、图 6)外, 细粒集合体草莓状黄铁矿和胶状闪锌矿具有明显负的 $\delta^{34}\text{S}$ 值(图 5f), 这表明该矿床还原态硫离子的形成除 TSR 过程外, 应该还存有别的形成过程或分馏机制。由于毛坪矿床成矿温度确实较高($> 180^\circ\text{C}$; 韩润生等, 2007), 不满足 BSR 过程在成矿阶段发生的温度条件。因此, 最合理的解释是 BSR 过程可能发生在成矿前, 即地层中富含石膏等海相硫酸盐的蒸发膏盐层在与富金属的成矿流体混合前, 由于温度低仅发生 BSR 过程, 产生少量还原态硫离子, 具有亏 $\delta^{34}\text{S}$ 特征, 形成少量细粒集合体草莓状黄铁矿和胶状闪锌矿。随着富金属流体与富硫流体混合程度的增加, 温度升高, BSR 过程终止, TSR 过程启动, 形成大量自形粒状黄铁矿和他形粒状闪锌矿。因此, 毛坪铅锌矿床还原态硫离子的形成过程经历了 BSR 和 TSR 过程, 这与该矿床硫源自原地海相蒸发膏盐层的认识是相互印证的。值得一提的是, 黄铁矿颗粒不同位置的原位 $\delta^{34}\text{S}$ 值略有差异, 表现为其中部较边

表 2 毛坪铅锌矿床方铅矿 fs LA-MC-ICPMS 原位 Pb 同位素组成

Table 2 The fs LA-MC-ICPMS in-situ Pb isotopic ratios of galena from the Maoping Pb-Zn deposit

测点号	样品位置	$\frac{^{206}\text{Pb}}{^{204}\text{Pb}}$	1s	$\frac{^{207}\text{Pb}}{^{204}\text{Pb}}$	1s	$\frac{^{208}\text{Pb}}{^{204}\text{Pb}}$	1s	$\frac{^{208}\text{Pb}}{^{206}\text{Pb}}$	1s	$\frac{^{207}\text{Pb}}{^{206}\text{Pb}}$	1s
MP-28-01		18.763	0.002	15.790	0.002	39.490	0.007	2.1047	0.0001	0.84154	0.00003
MP-28-02		18.763	0.002	15.791	0.002	39.495	0.006	2.1047	0.0001	0.84155	0.00002
MP-28-03	II 矿体	18.761	0.002	15.788	0.002	39.484	0.006	2.1045	0.0001	0.84149	0.00002
MP-28-04	760m 中段	18.768	0.002	15.796	0.002	39.513	0.006	2.1052	0.0001	0.84165	0.00002
MP-28-05		18.766	0.002	15.795	0.002	39.508	0.007	2.1053	0.0001	0.84169	0.00003
MP-28-06		18.768	0.002	15.796	0.003	39.512	0.007	2.1054	0.0001	0.84168	0.00003
MP-44-01		18.715	0.002	15.789	0.002	39.404	0.006	2.1056	0.0001	0.84369	0.00002
MP-44-02		18.713	0.002	15.788	0.002	39.399	0.005	2.1055	0.0001	0.84369	0.00002
MP-44-03	I 矿体	18.714	0.003	15.791	0.003	39.409	0.007	2.1058	0.0001	0.84377	0.00003
MP-44-04	720m 中段	18.719	0.002	15.794	0.002	39.417	0.006	2.1058	0.0001	0.84372	0.00002
MP-44-05		18.721	0.002	15.792	0.002	39.420	0.006	2.1056	0.0001	0.84358	0.00002
MP-44-06		18.712	0.003	15.789	0.003	39.407	0.007	2.1060	0.0001	0.84376	0.00003
MP-44-07		18.713	0.002	15.786	0.002	39.400	0.007	2.1054	0.0001	0.84361	0.00002
MP-67-01		18.740	0.002	15.789	0.002	39.445	0.006	2.1050	0.0001	0.84258	0.00002
MP-67-02	II 矿体	18.739	0.002	15.788	0.002	39.447	0.006	2.1051	0.0001	0.84256	0.00002
MP-67-03	736m 中段	18.746	0.003	15.795	0.003	39.467	0.008	2.1055	0.0001	0.84265	0.00003
MP-67-04		18.740	0.002	15.791	0.003	39.454	0.007	2.1052	0.0001	0.84263	0.00003
MP-67-05		18.744	0.002	15.793	0.002	39.458	0.006	2.1054	0.0001	0.84263	0.00003

部富集重 S 同位素, 这暗示黄铁矿结晶过程中, 可能发生了硫同位素的动力学瑞利分馏 (Zhou et al., 2018b; 杨兴玉等, 2018)。综上, 本文认为通过硫化物精细的原位 S 同位素地球化学研究, 有望为全面和深入理解贱金属硫化物矿床中还原态硫离子的来源、形成过程和分馏机制等提供新的约束。

5.2 成矿金属的来源与流体演化

以往对毛坪铅锌矿床 Pb 同位素地球化学的研究比较薄弱, 得出成矿金属主要源于上地壳的认识也比较笼统 (申屠良义等, 2011)。区域上, 大量的研究认为, 这些铅锌矿床潜在金属源区主要有下伏元古代基底浅变质岩石、震旦-中二叠统赋矿沉积岩和上覆晚二叠世峨眉山玄武岩三大类已基本达成共识 (Zheng and Wang, 1991; 柳贺昌和林文达, 1999; Zhou et al., 2001, 2011; 黄智龙等, 2004; 李文博等, 2006; 周家喜等, 2010, 2012; Li et al., 2015, 2016; 金中国等, 2016; Tan et al., 2017; Wang et al., 2018), 但对三类潜在源区为不同铅锌矿床贡献成矿物质的方式和比例有不同认识 (Zhou et al., 2018a)。

由于 U 和 Th 在方铅矿中的含量很低, 其形成放射性成因 Pb 的占比可以忽略不计, 所以方铅矿的 Pb 同位素组成无需进行成矿年龄校正即可代表成矿流体的 Pb 同位素组成 (Zheng and Wang, 1991; Carr et al., 1995; Zhou et al., 2014a; 金中国等, 2016)。本次研究获得的毛坪铅锌矿床不同矿体及其不同位置方铅矿的原位 Pb 同位素组成变化范围很窄 (表 2), 表明该矿床成矿金属的来源较为单一或混合均一化程度很高 (黄智龙等, 2004; Zhou et al., 2018b, c)。由于上述三大类岩石中普通 Pb 含量较高, 在与成矿流体对比

时, 需要进行成矿年龄校正 (Carr et al., 1995; Zhou et al., 2014b)。尽管沈战武等 (2016) 报道了毛坪铅锌矿床闪锌矿 Rb-Sr 等时线年龄为 $321.7 \pm 5.8\text{ Ma}$, 但是区域上现有的地质和同位素年代学资料并不支持该年龄能代表成矿年龄, 而 $230 \sim 200\text{ Ma}$ 是川滇黔地区铅锌矿床形成的主要时期已被广泛接受 (蔺志永等, 2010; 毛景文等, 2012; Zhou et al., 2013a, b, 2015, 2018a; Zhang et al., 2015; 胡瑞忠等, 2016; Hu et al., 2017b)。加之笔者刚刚获得的毛坪铅锌矿床成矿期方解石 LA-MC-ICPMS 原位 U-Pb 年龄为 209 Ma (周家喜等, 未发表数据)。因此, 采用 200 Ma 作为成矿年龄对上述三大类岩石进行 Pb 同位素组成校正是合理的。

将毛坪铅锌矿床方铅矿原位 Pb 同位素组成与成矿年龄校正后的下伏基底浅变质岩石、赋矿泥盆-石炭系沉积岩和上覆晚二叠统峨眉山玄武岩的 Pb 同位素组成范围进行对比 (图 7a), 不难发现毛坪矿床方铅矿具有明显不同于峨眉山玄武岩的 Pb 同位素组成, 其落入赋矿沉积岩和基底岩石 Pb 同位素组成范围之间, 但更靠近赋矿沉积岩范围 (图 7a), 同时也介于上地壳和下地壳端元的现代 Pb 同位素组成范围之间 (图 7a, b)。因此, 本文认为毛坪铅锌矿床的成矿金属最可能是由赋矿沉积岩提供的, 但不能排除基底岩石 (包括峨眉山玄武岩) 的贡献。

在 $^{207}\text{Pb}/^{204}\text{Pb}$ - $^{206}\text{Pb}/^{204}\text{Pb}$ (图 8a)、 $^{208}\text{Pb}/^{204}\text{Pb}$ - $^{206}\text{Pb}/^{204}\text{Pb}$ (图 8b) 和 $^{208}\text{Pb}/^{206}\text{Pb}$ - $^{207}\text{Pb}/^{206}\text{Pb}$ (图 8c) 图解上, 不难发现采自不同矿体及其不同标高位置的方铅矿 (表 2), 其原位 Pb 同位素组成具有一定变化规律, 即随着标高升高, 方铅矿原位 Pb 同位素组成具有升高趋势, 暗示毛坪铅锌矿床成矿流体是逐渐演化的, 且随着成矿流体演化, 富放射性成因 Pb 的

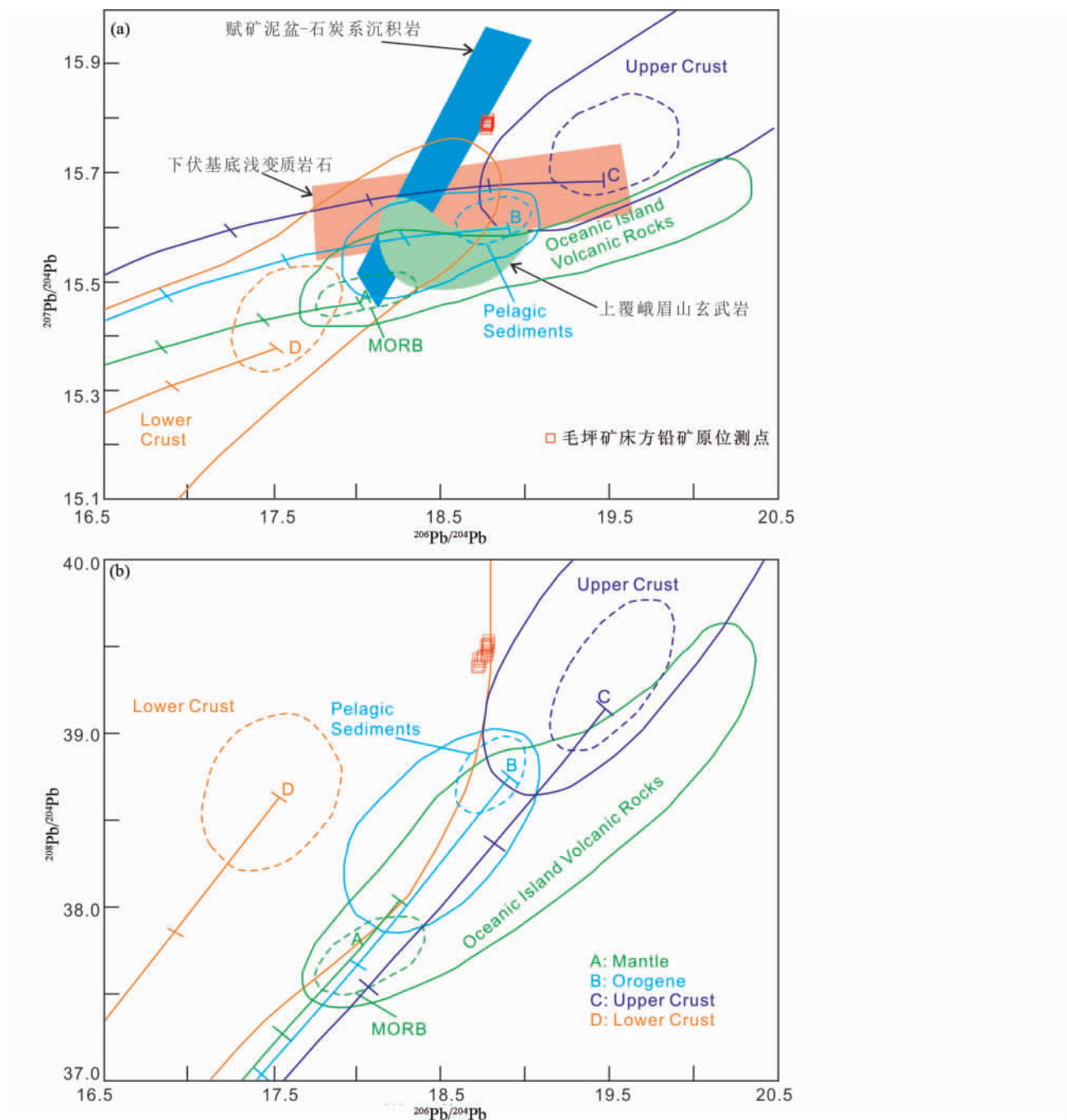


图 7 毛坪铅锌矿床方铅矿原位 Pb 同位素组成构造模式图(据 Zartman and Doe, 1981)

Fig. 7 Plots of $^{207}\text{Pb}/^{204}\text{Pb}$ vs. $^{206}\text{Pb}/^{204}\text{Pb}$ (a) and $^{208}\text{Pb}/^{204}\text{Pb}$ vs. $^{206}\text{Pb}/^{204}\text{Pb}$ (b) (after Zartman and Doe, 1981)

端元, 即赋矿沉积岩, 具有更显著的成矿物质贡献。由于赋矿沉积岩中 Pb、Zn 等成矿元素含量较低, 而基底岩石富含丰富的成矿元素(黄智龙等, 2004), 且研究区内铅锌矿床的成矿流体来源或流经基底岩石(Zhou et al. , 2018a), 所以本文推测基底岩石对毛坪矿床深部隐伏矿体的成矿物质贡献比例可能比浅部更大, 即越靠近深部的矿体, 其基底岩石贡献成矿物质的比例越大(如赋存于泥盆系宰格组中的 I 号矿体规模也最大)。因此, 毛坪铅锌矿床成矿流体是由下向上运

移和演化的, 这表明毛坪矿区深部具有良好的找矿潜力, 为下一步找矿预测指明了方向。

5.3 成矿过程

毛坪铅锌矿床三个主要矿体(群)赋存于不同层位(宰格组、摆佐组和威宁组)的白云岩之中, 受褶皱-层间构造控制明显(图 2、图 3), 矿化和蚀变具有较为明显的分带特征(魏爱英等, 2012; Wei et al. , 2015)。对毛坪大型铅锌矿床

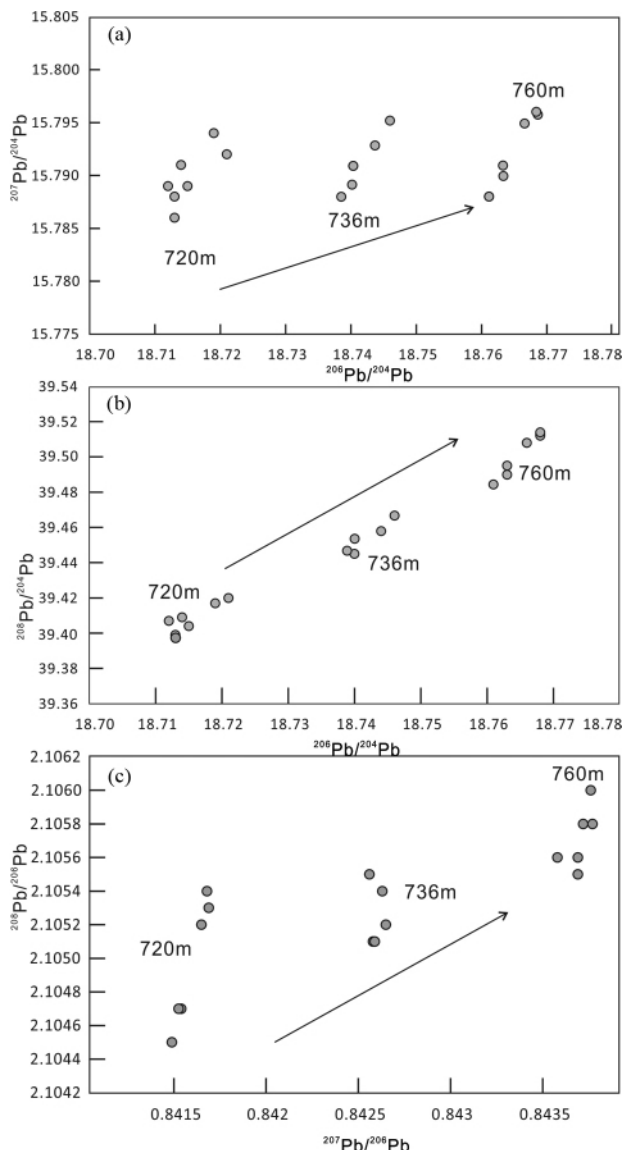


图8 毛坪铅锌矿床不同标高(720m、736m和760m)方铅矿原位Pb同位素组成变化特征

不同标高方铅矿 $^{207}\text{Pb}/^{204}\text{Pb}$ - $^{206}\text{Pb}/^{204}\text{Pb}$ 变化图(a)、 $^{208}\text{Pb}/^{204}\text{Pb}$ - $^{206}\text{Pb}/^{204}\text{Pb}$ 变化图(b)和 $^{208}\text{Pb}/^{206}\text{Pb}$ - $^{207}\text{Pb}/^{206}\text{Pb}$ 变化图(c)

Fig. 8 The variation characteristics of in-situ Pb isotopic ratios for different elevations galena in the Maoping Pb-Zn deposit

The variation plots of $^{207}\text{Pb}/^{204}\text{Pb}$ vs. $^{206}\text{Pb}/^{204}\text{Pb}$ (a), $^{208}\text{Pb}/^{204}\text{Pb}$ vs. $^{206}\text{Pb}/^{204}\text{Pb}$ (b) and $^{208}\text{Pb}/^{206}\text{Pb}$ vs. $^{207}\text{Pb}/^{206}\text{Pb}$ (c) for different elevations galena

是否属于MVT矿床,目前还有争议,例如张长青等(2005)认为包括毛坪矿床在内的川滇黔地区铅锌矿床均属于MVT矿床,而韩润生等(2012)则认为该矿床有别于MVT矿床,属于独特的“会泽式”矿床。由于毛坪矿床确实存在诸多有别于MVT矿床的成矿特征,如具有较高的矿石品位($\text{Pb} + \text{Zn} > 12\%$)、较高的成矿温度($> 180^\circ\text{C}$; 韩润生等, 2007)和较强

的蚀变-矿化分带特征(魏爱英等, 2012; Wei et al., 2015)等,强行将其归为MVT矿床或其亚类实有不妥,但毛坪铅锌矿床具有典型后生热液成矿特征是无疑的(图1-图4)。尽管本次工作并不能为毛坪铅锌矿床成因类型归属画上句号,但较为精细地刻画了其成矿过程,具体如下:

(1) 约260Ma,峨眉山地幔柱活动(Zhou et al., 2002)使得扬子板块西缘的古温度场比邻区高(约50°C; Zhou et al., 2018b),升高的热梯度背景加速了大规模深循环流体对流经岩石中成矿金属元素的活化、淋滤和萃取,进而形成富金属元素的成矿流体;

(2) 257~230Ma,早印支造山运动挤压驱动这些成矿流体沿着区域性构造(如昭通-曲靖隐伏断裂和垭都-紫云深大断裂等)大规模向上运移,沿途通过水/岩相互作用继续活化、淋滤和萃取流经地层沉积岩中的成矿金属元素,进而形成富金属元素的成矿混合流体(第一次富金属流体混合作用,形成的混合流体具有较高温度、富金属元素和贫硫等特征);

(3) 230~200Ma,印支造山运动晚期,扬子板块西缘构造背景从挤压转向伸展(Hu et al., 2017a, b; Zhou et al., 2018a),导致这些大规模富金属成矿混合流体向次级构造排泄,并被碳酸盐岩台地中的褶皱构造圈闭(如毛坪矿区的猫猫山背斜),与当地低温富 S^{2-} 和/or SO_4^{2-} 的层间建造流体或富石膏等海相硫酸盐的蒸发膏盐层发生第二次不同性质流体混合作用(即富金属流体与富硫流体的混合),启动TSR过程,最终导致矿石硫化物大量沉淀,形成工业矿体。在流体第二次混合成矿过程中,先消耗成矿前BSR过程产生的少量 S^{2-} (亏损 ^{34}S),形成细粒集合体草莓状黄铁矿和胶状闪锌矿的矿石,然后利用TSR过程形成的大量 S^{2-} (富集 ^{34}S),形成大量块状或稠密浸染状矿石。

需要指出的是,大量矿石硫化物的沉淀势必导致成矿热液体系的物理化学条件(如pH等)改变,而持续进行的成矿流体/围岩(水/岩)相互作用,可能起到重要的调节缓冲作用,即通过溶解-再结晶的碳酸盐矿物缓冲作用(Zhou et al., 2018c),来维持相对稳定有利的成矿物理化学条件。

6 结论

通过对毛坪大型铅锌矿床深入的矿床地质特征分析和系统的矿石硫化物原位S及Pb同位素地球化学研究,本文得出以下结论:

(1) 毛坪矿床主要受岩性和构造的双重控制,而与地层时代的关系并不明显;

(2) 毛坪矿床的硫源来自对应赋矿地层中富含石膏等海相硫酸盐的蒸发膏盐层,硫酸盐的还原经历了BSR和TSR过程,其中前者发生在富金属流体与富硫流体混合(即第二次不同性质流体混合)前,而后者发生在第二次不同性质流体混合后,不同性质流体第二次混合是导致TSR过程启动和

硫化物沉淀的重要机制;

(3) 毛坪矿床的成矿金属是由赋矿沉积岩提供, 但不排除下伏基底岩石(包括上覆峨眉山玄武岩)的贡献;

(4) 毛坪矿床成矿流体自下向上运移, 而富金属的基底岩石对下部矿体成矿物质的贡献比例更大, 暗示矿区深部具有一定的找矿潜力。

致谢 实验工作得到了中国科学院地质与地球物理研究所林杨挺研究员和张建超工程师及西北大学袁洪林教授和包志安工程师等的帮助; 成文过程中与中国科学院地球化学研究所温汉捷研究员、叶霖研究员和樊海峰研究员等进行了有益的讨论; 审稿人提出了诸多富有建设性的修改意见和建议; 在此对他们表示衷心的感谢!

References

- An Q, Zhou JX, Xu L, Yang XY, Ren HZ and Lu MD. 2018. A study of LA-MC-ICPMS in-situ Pb isotope geochemistry of the Maozhachang Pb-Zn deposit, NW Guizhou, China. *Acta Mineralogica Sinica*, 38 (6): 585–592 (in Chinese with English abstract)
- Bao Z, Yuan WT, Yuan HL, Liu X, Chen KY and Zong CL. 2016. Non-matrix-matched determination of lead isotope ratios in ancient bronze artifacts by femtosecond laser ablation multi-collector inductively coupled plasma mass spectrometry. *International Journal of Mass Spectrometry*, 402: 12–19
- Bao ZW, Li Q and Wang CY. 2017. Metal source of giant Huize Zn-Pb deposit in SW China: New constraints from in situ Pb isotopic compositions of galena. *Ore Geology Reviews*, 91: 824–836
- Basuki NI, Taylor BE and Spooner ETC. 2008. Sulfur isotope evidence for thermochemical reduction of dissolved sulfate in Mississippi Valley-type zinc-lead mineralization, Bongara area, northern Peru. *Economic Geology*, 103(4): 783–799
- Carr GR, Dean JA, Suppel DW and Heithersay PS. 1995. Precise lead isotope fingerprinting of hydrothermal activity associated with Ordovician to Carboniferous metallogenic events in the Lachlan fold belt of New South Wales. *Economic Geology*, 90(6): 1467–1505
- Chaussidon M, Albarède F and Sheppard SMF. 1989. Sulphur isotope variations in the mantle from ion microprobe analyses of micro-sulphide inclusions. *Earth and Planetary Science Letters*, 92(2): 144–156
- Chen W, Kong ZG, Liu FX, Wang XW, Deng MG, Zhao JX, Liu Y and Zhang XH. 2017. Geology, geochemistry ore and genesis of the Nayongzhi Pb-Zn deposit, Guizhou Province, NW China. *Acta Geologica Sinica*, 91(6): 1269–1284 (in Chinese with English abstract)
- Claypool GE, Holser WT, Kaplan IR, Sakai H and Zak I. 1980. The age curves of sulfur and oxygen isotopes in marine sulfate and their mutual interpretation. *Chemical Geology*, 28: 199–260
- Cui YL, Zhou JX, Huang ZL, Luo K, Nian HL, Ye L and Li ZL. 2018. Geology, geochemistry and ore genesis of the Fule Pb-Zn deposit, Yunnan Province, Southwest China. *Acta Petrologica Sinica*, 34 (1): 194–206 (in Chinese with English abstract)
- Gao S, Yang J, Zhou L, Li M, Hu ZC, Guo JL, Yuan HL, Gong HJ, Xiao GQ and Wei JQ. 2011. Age and growth of the Archean Kongling terrain, South China, with emphasis on 3.3Ga granitoid gneisses. *American Journal of Science*, 311(2): 153–182
- Han RS, Zou HJ, Hu B, Hu YZ and Xue CD. 2007. Features of fluid inclusions and sources of ore-forming fluid in the Maoping carbonate-hosted Zn-Pb-(Ag-Ge) deposit, Yunnan, China. *Acta Petrologica Sinica*, 23(9): 2109–2118 (in English)
- Han RS, Wang F, Zhao GS, Wang J, Zhou GM and Wang XK. 2010. New progress in deep prospecting of Zhaotong Maoping lead-zinc deposit, northeastern Yunnan Province metallogenic district. *Earth Science Frontiers*, 17(3): 275 (in Chinese)
- Han RS, Hu YZ, Wang XK, Hou BH, Huang ZL, Chen J, Wang F, Wu P, Li B, Wang HJ, Dong Y and Lei L. 2012. Mineralization model of rich Ge-Ag-bearing Zn-Pb polymetallic deposit concentrated district in northeastern Yunnan, China. *Acta Geologica Sinica*, 86 (2): 280–294 (in Chinese with English abstract)
- Hu RZ, Fu SL and Xiao JF. 2016. Major scientific problems on low-temperature metallogenesis in South China. *Acta Petrologica Sinica*, 32(11): 3239–3251 (in Chinese with English abstract)
- Hu RZ, Fu SL, Huang Y, Zhou MF, Fu SH, Zhao CH, Wang YJ, Bi XW and Xiao JF. 2017a. The giant South China Mesozoic low-temperature metallogenetic domain: Reviews and a new geodynamic model. *Journal of Asian Earth Sciences*, 137: 9–34
- Hu RZ, Chen WT, Xu DR and Zhou MF. 2017b. Reviews and new metallogenetic models of mineral deposits in South China: An introduction. *Journal of Asian Earth Sciences*, 137: 1–8
- Hua RM. 1994. Studies on metal deposition by fluid mixing during ore-forming processes. *Advance in Earth Sciences*, 9(4): 15–22 (in Chinese with English abstract)
- Huang ZL, Chen J, Liu CQ, Han RS, Li WB, Zhao DS, Gao DR and Feng ZH. 2001. A preliminary discussion on the genetic relationship between Emeishan basalts and Pb-Zn deposits as exemplified by the Huize Pb-Zn deposit, Yunnan Province. *Acta Mineralogica Sinica*, 21(4): 681–688 (in Chinese with English abstract)
- Huang ZL, Chen J, Han RS, Li WB, Liu CQ, Zhang ZL, Ma DY, Gao DR and Yang HL. 2004. Geochemistry and Ore-Formation of the Huize Giant Lead-Zinc Deposit, Yunnan Province, China: Discussion on the Relationship between the Emeishan Flood Basalts and Lead-Zinc Mineralization. Beijing: Geological Publishing House, 1–214 (in Chinese)
- Huang ZL, Li XB, Zhou MF, Li WB and Jin ZG. 2010. REE and C-O isotopic geochemistry of calcites from the world-class Huize Pb-Zn deposits, Yunnan, China: Implications for the ore genesis. *Acta Geologica Sinica*, 84(3): 597–613
- Huang ZL, Hu RZ, Su WC, Wen HJ, Liu S and Fu YZ. 2011. A study on the large-scale low-temperature metallogenetic domain in southwestern China: Significance, history and new progress. *Acta Mineralogica Sinica*, 31(3): 309–314 (in Chinese with English abstract)
- Jin RS, Zhang CJ, Feng XX, Tang C, Zhu Q and Li GY. 2014. The influence of fluid mixing on the mineralization of sandstone type uranium deposits. *Geological Bulletin of China*, 33(2–3): 354–358 (in Chinese)
- Jin ZG, Zhou JX, Huang ZL, Luo K, Gao JG, Peng S, Wang B and Chen XL. 2016. Ore genesis of the Nayongzhi Pb-Zn deposit, Puding City, Guizhou Province, China: Evidences from S and in situ Pb isotopes. *Acta Petrologica Sinica*, 32(11): 3441–3455 (in Chinese with English abstract)
- Jørgenson BB, Isachsen MF and Jannasch HW. 1992. Bacterial sulfate reduction above 100°C in deep-sea hydrothermal vent sediments. *Science*, 258(5089): 1756–1757
- Kong ZG, Wu Y, Liang T, Zhang F, Meng XY and Lu L. 2018. Sources of ore-forming material for Pb-Zn deposits in the Sichuan-Yunnan-Guizhou triangle area: Multiple constraints from C-H-O-S-Pb-Sr isotopic compositions. *Geological Journal*, 53(Suppl. 1): 159–177
- Leach DL, Sangster DF, Kelley KD, Large RR, Garven G, Allen CR, Guttmann J and Walters S. 2005. Sediment-hosted lead-zinc deposits: A global perspective. *Economic Geology* 100th Anniversary, SEG: 561–607
- Leach DL, Bradley DC, Huston D, Pisarevsky SA, Taylor RD and Gardoll SJ. 2010. Sediment-hosted lead-zinc deposits in Earth history. *Economic Geology*, 105(3): 593–625
- Li B, Zhou JX, Huang ZL, Yan ZF, Bao GP and Sun HR. 2015. Geological, rare earth elemental and isotopic constraints on the origin of the Banbanqiao Zn-Pb deposit, Southwest China. *Journal of Asian Earth Sciences*, 100: 1–12

- Earth Sciences, 111: 100–112
- Li B, Zhou JX, Li YS, Chen AB and Wang RX. 2016. Geology and isotope geochemistry of the Yinchanggou-Qiluogou Pb-Zn deposit, Sichuan Province, Southwest China. *Acta Geologica Sinica*, 90(5): 1768–1779
- Li WB, Huang ZL, Chen J, Han RS, Zhang ZL and Xu C. 2004. Rb-Sr dating of mineral assemblage from the Huize giant Zn-Pb deposit, Yunnan Province. *Acta Mineralogica Sinica*, 24(2): 112–116 (in Chinese with English abstract)
- Li WB, Huang ZL and Zhang G. 2006. Sources of the ore metals of the Huize ore field in Yunnan Province: Constraints from Pb, S, C, H, O and Sr isotope geochemistry. *Acta Petrologica Sinica*, 22(10): 2567–2580 (in Chinese with English abstract)
- Liang F, Bi XW, Feng CX, Tang YY, Wei DX and Dai ZH. 2016. Mineralogical and geochemical characteristics of carbonate and implications for ore-forming mechanism of the Fule Pb-Zn deposit, Yunnan Province, China. *Acta Petrologica Sinica*, 32(11): 3418–3430 (in Chinese with English abstract)
- Lin ZY, Wang DH and Zhang CQ. 2010. Rb-Sr isotopic age of sphalerite from the Paoma lead-zinc deposit in Sichuan Province and its implications. *Geology in China*, 37(2): 488–494 (in Chinese with English abstract)
- Liu HC and Lin WD. 1999. Study on the Law of Pb-Zn-Ag Ore Deposit in Northeast Yunnan, China. Kunming: Yunnan University Press, 1–468 (in Chinese)
- Liu JD, Zhang CJ, Liu XF, Yang ZX, Li YG and Wu DC. 2003. Discussion about relation between ore deposits of copper, lead, zinc, gold and silver in contiguous region between Sichuan, Yunnan and Guizhou provinces, and Emei igneous province. *Journal of Mineralogy and Petrology*, 23(4): 74–79 (in Chinese with English abstract)
- Liu WH, Zhang J and Wang J. 2017. Sulfur isotope analysis of carbonate-hosted Zn-Pb deposits in northwestern Guizhou Province, Southwest China: Implications for the source of reduced sulfur. *Journal of Geochemical Exploration*, 181: 31–44
- Luo K, Zhou JX, Huang ZL, Wang XC, Wilde SA, Zhou W and Tian L. 2019a. New insights into the origin of Early Cambrian carbonate-hosted Pb-Zn deposits in South China: A case study of the Maliping Pb-Zn deposit. *Gondwana Research*, 70: 88–103
- Luo K, Zhou JX, Huang ZL, Caulfield J, Zhao JX, Feng YX and Ouyang HG. 2019b. New insights into the evolution of MVT hydrothermal system: A case study of the Wusihe Pb-Zn deposit (South China), using quartz in situ trace elements and sulfides in situ S-Pb isotopes. *American Mineralogist*, doi: 10.2138/am-2020-7021
- Mao JW, Zhou ZH, Feng CY, Wang YT, Zhang CQ, Peng HJ and Yu M. 2012. A preliminary study of the Triassic large-scale mineralization in China and its geodynamic setting. *Geology in China*, 39(6): 1437–1471 (in Chinese with English abstract)
- Ohmoto H. 1972. Systematics of sulfur and carbon isotopes in hydrothermal ore deposits. *Economic Geology*, 67(5): 551–578
- Ohmoto H. 1986. Stable isotope geochemistry of ore deposits. *Reviews in Mineralogy and Geochemistry*, 16(1): 491–559
- Ohmoto H and Goldhaber MB. 1997. Sulfur and carbon isotopes. In: Barnes HL (ed.). *Geochemistry of Hydrothermal Ore Deposits*. 3rd Edition. New York: Wiley, 517–611
- Qin JH, Liao ZW, Zhu SB and Lai Y. 2016. Mineralization of the carbonate-hosted Pb-Zn deposits in the Sichuan-Yunnan-Guizhou area, southwestern China. *Sedimentary Geology and Tethyan Geology*, 36(1): 1–13 (in Chinese with English abstract)
- Qiu L, Yan DP, Tang SL, Wang Q, Yang WX, Tang XL and Wang JB. 2016. Mesozoic geology of southwestern China: Indosian foreland overthrusting and subsequent deformation. *Journal of Asian Earth Sciences*, 122: 91–105
- Qiu YM, Gao S, McNaughton NJ, Groves DI and Ling WL. 2000. First evidence of >3.2 Ga continental crust in the Yangtze craton of South China and its implications for Archean crustal evolution and Phanerozoic tectonics. *Geology*, 28(1): 11–14
- Ren SL, Li YH, Zeng PS, Qiu WL, Fan CF and Hu GY. 2018. Effect of sulfate evaporate salt layer in mineralization of the Huize and Maoping lead-zinc deposits in Yunnan: Evidence from sulfur isotope. *Acta Geologica Sinica*, 92(5): 1041–1055 (in Chinese with English abstract)
- Ren T, Zhou JX, Wang D, Yang GS and Lv CL. 2019. Trace elemental and S-Pb isotopic geochemistry of the Fule Pb-Zn deposit, NE Yunnan Province. *Acta Petrologica Sinica*, 35(11): 3493–3505 (in Chinese with English abstract)
- Rui ZY, Ye JH, Zhang LS, Wang LS and Mei YX. 2004. Pb-Zn deposits on the perimeter of the Yangtze craton and on the margins of its uplifts. *Geology in China*, 31(4): 337–346 (in Chinese with English abstract)
- Seal RR. 2006. Sulfur isotope geochemistry of sulfide minerals. *Reviews in Mineralogy and Geochemistry*, 61(1): 633–677
- Shen ZW, Jin CH, Dai YP, Zhang Y and Zhang H. 2016. Mineralization age of the Maoping Pb-Zn deposit in the northeastern Yunnan Province: Evidence from Rb-Sr isotopic dating of sphalerites. *Geological Journal of China Universities*, 22(2): 213–218 (in Chinese with English abstract)
- Shentu LY, Han RS, Li B and Qiu WL. 2011. Study on the isotope geochemistry of the Maoping Pb-Zn deposit, Zhaotong, Yunnan. *Mineral Resources and Geology*, 25(3): 211–216 (in Chinese with English abstract)
- Sun HR, Zhou JX, Huang ZL, Fan HF, Ye L, Luo K and Gao JG. 2016. The genetic relationship between Cu- and Zn-dominant mineralization in the Tianbaoshan deposit, Southwest China. *Acta Petrologica Sinica*, 32(11): 3407–3417 (in Chinese with English abstract)
- Tan SC, Zhou JX, Li B and Zhao JX. 2017. In situ Pb and bulk Sr isotope analysis of the Yinchanggou Pb-Zn deposit in Sichuan Province (SW China): Constraints on the origin and evolution of hydrothermal fluids. *Ore Geology Reviews*, 91: 432–443
- Tan SC, Zhou JX, Zhou MF and Ye L. 2019. In-situ S and Pb isotope constraints on an evolving hydrothermal system, Tianbaoshan Pb-Zn (Cu) deposit in South China. *Ore Geology Reviews*, 115: 103177
- Wang JZ, Li CY, Li ZQ and Liu JJ. 2001. The geological setting, characters and origin of Mississippi Valley-type Pb-Zn deposits in Sichuan and Yunnan provinces. *Geology-Geochemistry*, 29(2): 41–45 (in Chinese with English abstract)
- Wang JZ, Li CY, Li ZQ, Li BH and Liu WZ. 2002. The comparison of Mississippi Valley-type lead-zinc deposits in southwest of China and in mid-continent of United States. *Bulletin of Mineralogy, Petrology and Geochemistry*, 21(2): 127–132 (in Chinese with English abstract)
- Wang LJ, Mi M, Zhou JX and Luo K. 2018. New constraints on the origin of the Maozu carbonate-hosted epigenetic Zn-Pb deposit in NE Yunnan Province, SW China. *Ore Geology Reviews*, 101: 578–594
- Wei AY, Xue CD, Hong T, Luo DF, Li LR, Wang F, Zhou GM and Liu X. 2012. The alteration-mineralization zoning model for the Maoping lead-zinc deposit, northeastern Yunnan Province: Evidence from alteration-lithofacies mapping. *Acta Petrologica et Mineralogica*, 31(5): 723–735 (in Chinese with English abstract)
- Wei AY, Xue CD, Xiang K, Li J, Liao C and Akhter QJ. 2015. The ore-forming process of the Maoping Pb-Zn deposit, northeastern Yunnan, China: Constraints from cathodoluminescence (CL) petrography of hydrothermal dolomite. *Ore Geology Reviews*, 70: 562–577
- Wei WF, Hu RZ, Peng JT, Bi XW, Song SQ and Shi SH. 2011. Fluid mixing in Xihuashan tungsten deposit, southern Jiangxi Province: Hydrogen and oxygen isotope simulation analysis. *Geochimica*, 40(1): 45–55 (in Chinese with English abstract)
- Wu Y, Zhang CQ, Mao JW, Ouyang HG and Sun J. 2013. The genetic relationship between hydrocarbon systems and Mississippi Valley-type Zn-Pb deposits along the SW margin of Sichuan Basin, China. *International Geology Review*, 55(8): 941–957
- Xu YK, Huang ZL, Zhu D and Luo TY. 2014. Origin of hydrothermal

- deposits related to the Emeishan magmatism. *Ore Geology Reviews*, 63: 1–8
- Yang XY, Zhou JX, An Q, Ren HZ, Xu L, Lu MD and Wu CJ. 2018. Formation mechanism of reduced S in the Nayongzhi Pb-Zn deposit, Guizhou Province, China: Constraint from the NanoSIMS in-situ S isotopes. *Acta Mineralogica Sinica*, 38(6): 593–599 (in Chinese with English abstract)
- Yuan HL, Yin C, Liu X, Chen KY, Bao ZA, Zong CL, Dai MN, Lai SC, Wang R and Jiang SY. 2015. High precision in-situ Pb isotopic analysis of sulfide minerals by femtosecond laser ablation multi-collector inductively coupled plasma mass spectrometry. *Science China (Earth Sciences)*, 58(10): 1713–1721
- Yuan HL, Yuan WT, Cheng C, Liang P, Liu X, Dai MN, Bao ZA, Zong CL, Chen KY and Lai SC. 2016. Evaluation of lead isotope compositions of NIST NBS 981 measured by thermal ionization mass spectrometer and multiple-collector inductively coupled plasma mass spectrometer. *Solid Earth Sciences*, 1(2): 74–78
- Zartman RE and Doe BR. 1981. Plumbotectonics: The model. *Tectonophysics*, 75(1–2): 135–162
- Zhang CQ, Mao JW, Wu SP, Li HM, Liu F, Guo BJ and Gao DR. 2005. Distribution, characteristics and genesis of Mississippi Valley-type lead-zinc deposits in Sichuan-Yunnan-Guizhou area. *Mineral Deposits*, 24(3): 336–348 (in Chinese with English abstract)
- Zhang CQ, Rui ZY, Chen YC, Wang DH, Chen ZH and Lou DB. 2013. The main successive strategic bases of resources for Pb-Zn deposits in China. *Geology in China*, 40(1): 248–272 (in Chinese with English abstract)
- Zhang CQ, Wu Y, Hou L and Mao JW. 2015. Geodynamic setting of mineralization of Mississippi Valley-type deposits in world-class Sichuan-Yunnan-Guizhou Zn-Pb triangle, Southwest China: Implications from age-dating studies in the past decade and the Sm-Nd age of Jinshachang deposit. *Journal of Asian Earth Sciences*, 103: 103–114
- Zhang JC, Lin YT, Yang W, Shen WJ, Hao JL, Hu S and Cao MJ. 2014. Improved precision and spatial resolution of sulfur isotope analysis using NanoSIMS. *Journal of Analytical Atomic Spectrometry*, 29(10): 1934–1943
- Zhang ZB, Li CY, Tu GC, Xia B and Wei ZQ. 2006. Geotectonic evolution background and ore-forming process of Pb-Zn deposits in Chuan-Dian-Qian area of Southwest China. *Geotectonica et Metallogenesis*, 30(3): 343–354 (in Chinese with English abstract)
- Zhao XF, Zhou MF, Li JW, Sun M, Gao JF, Sun WH and Yang JH. 2010. Late Paleoproterozoic to Early Mesoproterozoic Dongchuan Group in Yunnan, SW China: Implications for tectonic evolution of the Yangtze Block. *Precambrian Research*, 182(1–2): 57–69
- Zheng MH and Wang XC. 1991. Ore genesis of the Daliangzi Pb-Zn deposit in Sichuan, China. *Economic Geology*, 86(4): 831–846
- Zhou CX, Wei CS and Guo JY. 2001. The source of metals in the Qilinchang Zn-Pb deposit, northeastern Yunnan, China: Pb-Sr isotope constraints. *Economic Geology*, 96(3): 583–598
- Zhou JX, Huang ZL, Zhou GF, Jin ZG, Li XB, Ding W and Gu J. 2010. Sources of the ore metals of the Tianqiao Pb-Zn deposit in northwestern Guizhou Province: Constraints from S, Pb isotope and REE geochemistry. *Geological Review*, 56(4): 513–524 (in Chinese with English abstract)
- Zhou JX, Huang ZL, Zhou GF, Li XB, Ding W and Bao GP. 2011. Trace elements and rare earth elements of sulfide minerals in the Tianqiao Pb-Zn ore deposit, Guizhou Province, China. *Acta Geologica Sinica*, 85(1): 189–199
- Zhou JX, Huang ZL, Zhuo GF and Zeng QS. 2012. C, O isotope and REE geochemistry of the hydrothermal calcites from the Tianqiao Pb-Zn ore deposit in NW Guizhou Province, China. *Geotectonica et Metallogenesis*, 36(1): 93–101 (in Chinese with English abstract)
- Zhou JX, Huang ZL, Zhou MF, Li XB and Jin ZG. 2013a. Constraints of C-O-S-Pb isotope compositions and Rb-Sr isotopic age on the origin of the Tianqiao carbonate-hosted Pb-Zn deposit, SW China. *Ore Geology Reviews*, 53: 77–92
- Zhou JX, Huang ZL and Bao GP. 2013b. Geological and sulfur-lead-strontium isotopic studies of the Shaojiwan Pb-Zn deposit, Southwest China: Implications for the origin of hydrothermal fluids. *Journal of Geochemical Exploration*, 128: 51–61
- Zhou JX, Huang ZL, Gao JG and Yan ZF. 2013c. Geological and C-O-S-Pb-Sr isotopic constraints on the origin of the Qingshan carbonate-hosted Pb-Zn deposit, Southwest China. *International Geology Review*, 55(7): 904–916
- Zhou JX, Huang ZL and Yan ZF. 2013d. The origin of the Maozu carbonate-hosted Pb-Zn deposit, Southwest China: Constrained by C-O-S-Pb isotopic compositions and Sm-Nd isotopic age. *Journal of Asian Earth Sciences*, 73: 39–47
- Zhou JX, Huang ZL, Bao GP and Gao JG. 2013e. Sources and thermo-chemical sulfate reduction for reduced sulfur in the hydrothermal fluids, southeastern SYG Pb-Zn metallogenic province, SW China. *Journal of Earth Science*, 24(5): 759–771
- Zhou JX, Huang ZL, Zhou MF, Zhu XK and Muchez P. 2014a. Zinc, sulfur and lead isotopic variations in carbonate-hosted Pb-Zn sulfide deposits, Southwest China. *Ore Geology Reviews*, 58: 41–54
- Zhou JX, Huang ZL, Lv ZC, Zhu XK, Gao JG and Mirnejad H. 2014b. Geology, isotope geochemistry and ore genesis of the Shanshulin carbonate-hosted Pb-Zn deposit, Southwest China. *Ore Geology Reviews*, 63: 209–225
- Zhou JX, Bai JH, Huang ZL, Zhu D, Yan ZF and Lv ZC. 2015. Geology, isotope geochemistry and geochronology of the Jinshachang carbonate-hosted Pb-Zn deposit, Southwest China. *Journal of Asian Earth Sciences*, 98: 272–284
- Zhou JX, Luo K, Li B, Huang ZL and Yan ZF. 2016a. Geological and isotopic constraints on the origin of the Anle carbonate-hosted Zn-Pb deposit in northwestern Yunnan Province, SW China. *Ore Geology Reviews*, 74: 88–100
- Zhou JX, Dou S, Huang ZL, Cui YL, Ye L, Li B, Gan T and Sun HR. 2016b. Origin of the Luping Pb deposit in the Beiya area, Yunnan Province, SW China: Constraints from geology, isotope geochemistry and geochronology. *Ore Geology Reviews*, 72: 179–190
- Zhou JX, Xiang ZZ, Zhou MF, Feng YX, Luo K, Huang ZL and Wu T. 2018a. The giant Upper Yangtze Pb-Zn province in SW China: Reviews, new advances and a new genetic model. *Journal of Asian Earth Sciences*, 154: 280–315
- Zhou JX, Luo K, Wang XC, Wilde SA, Wu T, Huang ZL, Cui YL and Zhao JX. 2018b. Ore genesis of the Fule Pb-Zn deposit and its relationship with the Emeishan Large Igneous Province: Evidence from mineralogy, bulk C-O-S and in situ S-Pb isotopes. *Gondwana Research*, 54: 161–179
- Zhou JX, Wang XC, Wilde SA, Luo K, Huang ZL, Wu T and Jin ZG. 2018c. New insights into the metallogeny of MVT Zn-Pb deposits: A case study from the Nayongzhi in South China, using field data, fluid compositions, and in situ S-Pb isotopes. *American Mineralogist*, 103(1): 91–108
- Zhou MF, Malpas J, Song XY, Robinson PT, Sun M, Kennedy AK, Lesher CM and Keays RR. 2002. A temporal link between the Emeishan large igneous province (SW China) and the end-Guadalupian mass extinction. *Earth and Planetary Science Letters*, 196(3–4): 113–122
- Zhu CW, Wen HJ, Zhang YX and Fan HF. 2016. Cadmium and sulfur isotopic compositions of the Tianbaoshan Zn-Pb-Cd deposit, Sichuan Province, China. *Ore Geology Reviews*, 76: 152–162
- Zhu CW, Wen HJ, Zhang YX, Fu SH, Fan HF and Cloquet C. 2017. Cadmium isotope fractionation in the Fule Mississippi Valley-type deposit, Southwest China. *Mineralium Deposita*, 52(5): 675–686
- Zou HJ, Han RS, Hu B and Liu H. 2004. New evidences of origin of metallogenic materials in the Maoping Pb-Zn ore deposit, Zhaotong, Yunnan: R-factor analysis results of trace elements in NE-extending fractural tectonites. *Geology and Prospecting*, 40(5): 43–48 (in Chinese with English abstract)

附中文参考文献

安琦, 周家喜, 徐磊, 杨兴玉, 任厚州, 卢贺达. 2018. 黔西北猫樟

- 厂铅锌矿床原位 Pb 同位素地球化学. 矿物学报, 38(6) : 585 – 592
- 陈伟, 孔志岗, 刘凤祥, 王学武, 邓明国, 赵剑星, 刘阳, 张兴华. 2017. 贵州纳雍枝铅锌矿床地质、地球化学及矿床成因. 地质学报, 91(6) : 1269 – 1284
- 崔银亮, 周家喜, 黄智龙, 罗开, 念红良, 叶霖, 李珍立. 2018. 云南富乐铅锌矿床地质、地球化学及成因. 岩石学报, 34(1) : 194 – 206
- 韩润生, 邹海俊, 胡彬, 胡煜昭, 薛传东. 2007. 云南毛坪铅锌(银、锗) 矿床流体包裹体特征及成矿流体来源. 岩石学报, 23(9) : 2109 – 2118
- 韩润生, 王峰, 赵高山, 王进, 周高明, 王学琨. 2010. 滇东北富集区昭通毛坪铅锌矿床深部找矿新进展. 地学前缘, 17(3) : 275
- 韩润生, 胡煜昭, 王学琨, Hou BH, 黄智龙, 陈进, 王峰, 吴鹏, 李波, 王洪江, 董英, 雷丽. 2012. 滇东北富锗银铅锌多金属矿集区矿床模型. 地质学报, 86(2) : 280 – 294
- 胡瑞忠, 付山岭, 肖加飞. 2016. 华南大规模低温成矿的主要科学问题. 岩石学报, 32(11) : 3239 – 3251
- 华仁民. 1994. 成矿过程中由流体混合而导致金属沉淀的研究. 地球科学进展, 9(4) : 15 – 22
- 黄智龙, 陈进, 刘丛强, 韩润生, 李文博, 赵德顺, 高德荣, 冯志宏. 2001. 峨眉山玄武岩与铅锌矿床成矿关系初探——以云南会泽铅锌矿床为例. 矿物学报, 21(4) : 681 – 688
- 黄智龙, 陈进, 韩润生, 李文博, 刘丛强, 张振亮, 马德云, 高德荣, 杨海林. 2004. 云南会泽超大型铅锌矿床地球化学及成因——兼论峨眉山玄武岩与铅锌成矿的关系. 北京: 地质出版社, 1 – 214
- 黄智龙, 胡瑞忠, 苏文超, 温汉捷, 刘燊, 符亚洲. 2011. 西南大面积低温成矿域: 研究意义、历史及新进展. 矿物学报, 31(3) : 309 – 314
- 金若时, 张成江, 冯晓曦, 汤超, 朱强, 李光耀. 2014. 流体混合对砂岩型铀矿成矿作用的影响. 地质通报, 33(2 – 3) : 354 – 358
- 金中国, 周家喜, 黄智龙, 罗开, 高建国, 彭松, 王兵, 陈兴龙. 2016. 贵州普定纳雍枝铅锌矿床成因: S 和原位 Pb 同位素证据. 岩石学报, 32(11) : 3441 – 3455
- 李文博, 黄智龙, 陈进, 韩润生, 张振亮, 许成. 2004. 会泽超大型铅锌矿床成矿时代研究. 矿物学报, 24(2) : 112 – 116
- 李文博, 黄智龙, 张冠. 2006. 云南会泽铅锌矿田成矿物质来源: Pb、S、C、H、O、Sr 同位素制约. 岩石学报, 22(10) : 2567 – 2580
- 梁峰, 毕献武, 冯彩霞, 唐永永, 韦东晓, 戴智慧. 2016. 云南富乐铅锌矿床碳酸盐矿物化学特征及其对成矿作用的指示. 岩石学报, 32(11) : 3418 – 3430
- 蔺志永, 王登红, 张长青. 2010. 四川宁南跑马铅锌矿床的成矿时代及其地质意义. 中国地质, 37(2) : 488 – 494
- 柳贺昌, 林文达. 1999. 滇东北铅锌银矿床规律研究. 昆明: 云南大学出版社, 1 – 468
- 刘家铎, 张成江, 刘显凡, 阳正熙, 李佑国, 吴德超. 2003. 川滇黔相邻区域铜铅锌金银矿床与峨眉火成岩省的关系探讨. 矿物岩石, 23(4) : 74 – 79
- 毛景文, 周振华, 丰成友, 王义天, 张长青, 彭惠娟, 于森. 2012. 初论中国三叠纪大规模成矿作用及其动力学背景. 中国地质, 39(6) : 1437 – 1471
- 秦建华, 廖震文, 朱斯豹, 赖杨. 2016. 川滇黔相邻区碳酸盐岩容矿铅锌矿成矿特征. 沉积与特提斯地质, 36(1) : 1 – 13
- 任顺利, 李延河, 曾普胜, 邱文龙, 范昌福, 胡古月. 2018. 腺盐层在云南会泽和毛坪铅锌矿成矿中的作用: 硫同位素证据. 地质学报, 92(5) : 1041 – 1055
- 任涛, 周家喜, 王蝶, 杨光树, 吕昶良. 2019. 滇东北富乐铅锌矿床微量元素和 S-Pb 同位素地球化学研究. 岩石学报, 35(11) : 3493 – 3505
- 芮宗瑶, 叶锦华, 张立生, 王龙生, 梅燕雄. 2004. 扬子克拉通周边及其隆起边缘的铅锌矿床. 中国地质, 31(4) : 337 – 346
- 沈战武, 金灿海, 代堰培, 张玙, 张海. 2016. 滇东北毛坪铅锌矿床的成矿时代: 闪锌矿 Rb-Sr 定年. 高校地质学报, 22(2) : 213 – 218
- 申屠良义, 韩润生, 李波, 邱文龙. 2011. 云南昭通毛坪铅锌矿床同位素地球化学性质研究. 矿产与地质, 25(3) : 211 – 216
- 孙海瑞, 周家喜, 黄智龙, 樊海峰, 叶霖, 罗开, 高建国. 2016. 四川会理天宝山矿床深部新发现铜矿与铅锌矿的成因关系探讨. 岩石学报, 32(11) : 3407 – 3417
- 王奖臻, 李朝阳, 李泽琴, 刘家军. 2001. 川滇地区密西西比河谷型铅锌矿床成矿地质背景及成因探讨. 地质地球化学, 29(2) : 41 – 45
- 王奖臻, 李朝阳, 李泽勤, 李葆华, 刘文周. 2002. 川、滇、黔交界地区密西西比河谷型铅锌矿床与美国同类矿床的对比. 矿物岩石地球化学通报, 21(2) : 127 – 132
- 魏爱英, 薛传东, 洪托, 罗大峰, 李炼然, 王锋, 周高明, 刘星. 2012. 滇东北毛坪铅锌矿床的蚀变-矿化分带模式——蚀变岩相填图证据. 岩石矿物学杂志, 31(5) : 723 – 735
- 魏文凤, 胡瑞忠, 彭建堂, 毕献武, 宋生琼, 石少华. 2011. 赣南西华山钨矿床的流体混合作用: 基于 H、O 同位素模拟分析. 地球化学, 40(1) : 45 – 55
- 杨兴玉, 周家喜, 安琦, 任厚州, 徐磊, 卢贺达, 吴才进. 2018. 贵州纳雍枝铅锌矿床还原 S 的形成机制: NanoSIMS 原位 S 同位素约束. 矿物学报, 38(6) : 593 – 599
- 张长青, 毛景文, 吴锁平, 李厚民, 刘峰, 郭保健, 高德荣. 2005. 川滇黔地区 MVT 铅锌矿床分布、特征及成因. 矿床地质, 24(3) : 336 – 348
- 张长青, 芮宗瑶, 陈毓川, 王登红, 陈郑辉, 娄德波. 2013. 中国铅锌矿资源潜力和主要战略接续区. 中国地质, 40(1) : 248 – 272
- 张志斌, 李朝阳, 涂光炽, 夏斌, 韦振权. 2006. 川、滇、黔接壤地区铅锌矿床产出的大地构造演化背景及成矿作用. 大地构造与成矿学, 30(3) : 343 – 354
- 周家喜, 黄智龙, 周国富, 金中国, 李晓彪, 丁伟, 谷静. 2010. 黔西北赫章天桥铅锌矿床成矿物质来源: S、Pb 同位素和 REE 制约. 地质论评, 56(4) : 513 – 524
- 周家喜, 黄智龙, 周国富, 曾乔松. 2012. 黔西北天桥铅锌矿床热液方解石 C、O 同位素和 REE 地球化学. 大地构造与成矿学, 36(1) : 93 – 101
- 邹海俊, 韩润生, 胡彬, 刘鸿. 2004. 云南昭通毛坪铅锌矿床成矿物质来源的新证据——NE 向断裂构造岩微量元素 R 型因子分析结果. 地质与勘探, 40(5) : 43 – 48